5. Spikes and Transition-Layers: Piece-wise Linear Models

Two mechanisms for transition between quasi-steady patterns in sequences generated on the slowly growing domain are observed for the kinetic models in the literature admitting DDI. In the previous chapter these mechanisms were illustrated with Schnakenberg kinetics for activator peak splitting, shown in Figure 4.1(a), and by the Gierer-Meinhardt model for peak insertion, see Figure 4.10(a). In this chapter we seek to understand these properties of the equations and in particular establish what determines the mode of transition for a particular choice of kinetic scheme. To these ends we simplify the problem by introducing a piece-wise linear approximation to the reaction-diffusion system.

In Chapter 4 it was shown that for slow domain growth the evolution of solutions to the PDE separates into two distinct timescales. Here we make use of this separation of scales and consider the parameterisation by γ of quasi-steady patterns which evolve on the slow timescale. In the limit as ρ tends to zero these patterns are well approximated by the steady state patterns for the reaction-diffusion equation on the fixed domain. Furthermore, for small d the spatial behaviour of the reaction-diffusion system is separated into regions where the solution varies on two distinct spatial scales. It is convenient to write $d \equiv \epsilon^2$ where $\epsilon \ll 1$. Then in the limit $\epsilon \to 0$ the spatial variation of solutions in the steady state is determined by the *outer* equations

$$u_{xx} = -\gamma f(u,v) \tag{5.1}$$

$$0 = g(u,v) \tag{5.2}$$

suggesting that the solution must lie on the nullcline for v, except in the vicinity of large spatial gradients in v, where we expand the independent variable, $\xi = x/\epsilon$, to obtain the *inner* approximation

$$u_{\xi\xi} = 0 \tag{5.3}$$

$$v_{\xi\xi} = -\gamma g(u,v). \tag{5.4}$$

Our method is to exploit the ratio of diffusivities d as a small parameter in a singular perturbation expansion in which we look for solutions in the limit as d tends to zero. In particular we can find closed form approximate solutions of the system, showing that the slow dynamics carry the system to a point, which can be calculated, where a solution of a given mode ceases to exist and where reorganisation of the pattern ensues on the fast timescale. From this analysis we also identify a novel behaviour, *frequency-tripling*, which is characteristic of a symmetry in the kinetic equations.

The steady patterns arising from the Turing instability in reaction-diffusion equations may be grouped into two classes, according to the asymptotic behaviour as the

ratio of diffusivities tends to zero. *Spike* patterns, such as those generated by the Schnakenberg and Gierer-Meinhardt systems, consist of periodic peaks in the activator profile for which the amplitude increases (and becomes unbounded) and the width decreases as d is reduced to zero. Thus spike patterns approximate δ-functions in the limit. *Transition-layer* patterns develop discontinuous jumps between two activator levels, becoming step-functions as d tends to zero. The difference between these two pattern-types is determined by the manner in which the kinetics saturate the growth of destabilising modes, in particular by the shape of the nullcline for the activator kinetics (see, for example, Kerner and Osipov [62]—we take a similar approach to theirs below).

Reaction-diffusion models for spatial patchiness in population levels for predator-prey interactions have been proposed by Segel and Jackson [121] and Levin and Segel [73], in which the spatial distribution is generated by DDI. In many such ecological settings it is desirable that the subdivision of the domain into regions of high and low population density is maintained when the prey species is effectively stationary, such as herbivore-plant interactions (herbivorous copepods, zooplankton, and grazing phytoplankton [73]) or various host-parasite systems [121]. In this case the ratio of prey to predator diffusivity is reduced to zero. Mimura and Murray [83] showed that for these models the spatial extent of regions of high population tended to zero with the ratio of diffusivities (the kinetics are spike-type), and proposed that a cubic form is required for the nullclines for pattern which continues to subdivide the domain as d is decreased.

Much of the theory of large amplitude patterns of transition-layer type was developed by Fife [39, 40]. Kerner and Osipov discuss these patterns and their stability [62] and also discuss spike-type kinetics. Spike patterns, or point condensations, are the subject of much current interest (see Ni [92] for a recent review). Doelman and co-workers have used geometric singular perturbation theory to investigate the existence [33] and stability [32] of spike patterns in the Gray-Scott model, also studied by Muratov and Osipov [86]. Alternatively, Ward *et al.* [53, 54] consider the stability of spike solutions to the Gierer-Meinhardt system and the motion of spike solutions in two and three dimensions.

5.1 Transition-Layer Theory

Fife [38] showed the existence of large amplitude stationary solutions in a class of coupled reaction-diffusion equations, characterised by narrow transition regions which subdivide the domain into two phases (high and low activator concentrations), requiring one component to diffuse much faster that the other. Fife's discussion of these solutions depends on global properties of the system, rather than on the local behaviour of the system close to a bifurcation point, as do Turing's analysis and the weakly nonlinear bifurcation analysis presented in Chapter 2. Large amplitude weak solutions to the steady state problem may be constructed in the limiting case $\epsilon = 0$ by

allowing a jump discontinuity in the solution, which for $\epsilon \neq 0$ is smoothed out to give a continuously differentiable graph. In the singular limit solutions are deemed *weak* as they admit a jump discontinuity. In comparison to a bifurcation-type approach, here we are nowhere near a fixed point in phase space. In fact the conditions derived for Turing bifurcation from a homogeneous state, described in Chapter 2, are not necessary requirements. Large amplitude solutions may be formed where a sufficiently strong perturbation from a stable fixed point in the phase space takes the solution to a branch of stationary inhomogeneous solutions, so-called Turing branches, as discussed for the bistable Gray-Scott model in section 2.5.3.

The argument we present below is based in part on a discussion in the book by Grindrod [46], where a population model for ecological patchiness (predator-prey type interaction with diffusion) is considered. Conway [18] has a fuller discussion (see also Murray and Mimura [83]). In this chapter we use singular perturbation theory to construct heterogeneous solutions, showing existence of large amplitude patterns for a concrete example, and then examine the dependence of these solutions on γ. We will not pursue the analytical study of stability of the solutions, but rather refer to the arguments presented for transition-layer solutions by Fife [39] and also the work of Kerner and Osipov [62].

Transition-layer patterns may form in systems for which the activator nullcline takes a cubic form in the (u, v) phase plane, so that $g(u, v) = 0$ must have three solutions $v = k(u)$. The shape of the inhibitor nullcline $f = 0$ is not crucial for the existence of large amplitude patterns as long as the kinetics are monostable (such that the curves $f = 0$ and $g = 0$ intersect only at one point). We will discuss variations of this nullcline later. The two essential ingredients are the specific form of the activator nullcline and that the ratio of diffusivities is a small parameter. Below we illustrate the basic idea and show how it helps understand splitting and insertion. In a following section we pursue a specific example, where the analysis has been dramatically simplified by assuming a piece-wise linear form for the kinetics.

We study the coupled reaction-diffusion system for two species

$$u_t = \frac{1}{\gamma} u_{xx} + f(u, v) \tag{5.5}$$

$$v_t = \frac{\epsilon^2}{\gamma} v_{xx} + g(u, v) \tag{5.6}$$

with zero flux boundary conditions

$$u_x = v_x = 0 \quad \text{on} \quad x = 0, 1 \tag{5.7}$$

where the nullcline $g = 0$ has cubic form. The steady states of this equation are equivalent to the quasi-steady patterns for the problem on a growing domain, given by equations (4.9)–(4.10).

First we consider the possibility of solutions when $\epsilon = 0$. Consider the activator kinetics

$$v_t = g(u, v), \tag{5.8}$$

which has three stationary branches (the nullcline $g(u, v) = 0$) in the phase space, $v = k_i(u)$ where $i = 1, 2, 3$. In order to have transitions between two phases (corresponding to two branches of the nullcline) it must be the case that two of the branches, $i = 1$ and 3, are stable with respect to the dynamical system (5.8), for which we require $g_v < 0$. Following our ordering of the species in decreasing diffusivity, for DDI we must have $g_v > 0$ (self-activation of v) at the fixed point of the kinetics, which for consistency must lie on the unstable branch.[1] However, we note that the existence of the large amplitude transition-layer patterns does not depend on this condition, and below we discuss the implications of the kinetic steady state lying elsewhere. Simple considerations on the gradient of the nullcline at the fixed point (branch $i = 2$) dictate that for pure kinetics the nullcline is a negative cubic in v while for cross kinetics the nullcline has positive cubic form.

Firstly we consider the case of pure kinetics for which the nullcline is a negative cubic function of v, and so k_1 is defined on $u \in [u_{min}, \infty)$ while k_2 is defined on $u \in [u_{min}, u_{max}]$ and k_3 on $u \in (-\infty, u_{max}]$. Here u_{min} and u_{max} are the values of u at the turning points of the curve $g(u, v) = 0$ in the phase plane. From the phase plane it is straightforward to show that there are no nontrivial solutions with $v = k_i(u)$ satisfying both the conditions imposed at the boundaries. Next we consider solutions which are continuous in $u(x)$ and its derivative $u_x(x)$ but which allow a discontinuity in $v(x)$ at $x = x^* \in [0, 1]$ where $u = u^* \in [u_{min}, u_{max}]$ satisfying the reduced system

$$0 = u_{xx} + \gamma h(u) \tag{5.9}$$

where

$$h(u) = \begin{cases} f(u, k_1(u)), & u < u^* \\ f(u, k_3(u)), & u > u^* \end{cases} \tag{5.10}$$

and for a pure system $f(u, k_1(u)) < 0$ and $f(u, k_3(u)) > 0$ (for cross kinetics the signs are reversed). Assuming monostability, $h(u)$ has no roots ($f(u, k_2(u)) = 0$ at $u = u_s$ which is on branch $i = 2$). We look for orbits of this equation in the phase plane starting and finishing on $u_x = 0$. A schematic of a typical phase plane for equation (5.9) is shown in Figure 5.1. Here we construct a solution such that $v = k_1(u)$ for $0 \le x < x^*$ and $v = k_3(u)$ for $x^* < x \le 1$. Evidently we could reverse the polarity, and jump from branch $i = 3$ to branch $i = 1$ as x increases, for which we would have

[1] We note that the so-called 'unstable' branch ($i = 2$) is unstable *w.r.t.* equation (5.8), however, it is consistent that the fixed point of the kinetics (u_s, v_s) which lies on this branch is stable *w.r.t.* the dynamical system $u_t = f(u, v)$, $v_t = g(u, v)$, as required in the definition of the Turing bifurcation (and may be driven unstable by spatially heterogeneous perturbation for the full reaction-diffusion equation).

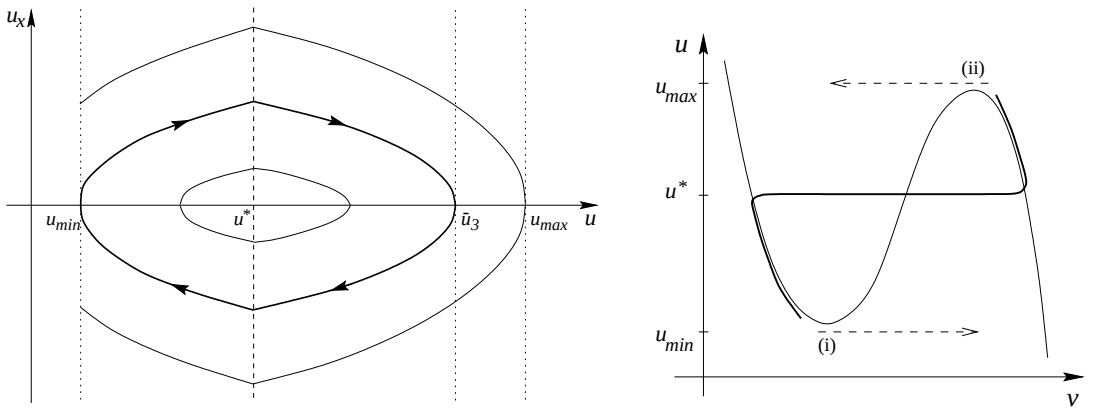

(a) (b)

FIGURE 5.1 Schematics of (a) the phase plane for equation (5.9), the outer problem for transition-layer patterns, and (b) the solution (bold) and the curve $g(u,v)=0$, showing the solution lying on the nullcline away from the jump in v at $u=u^*$ and the limiting points corresponding to case (i) and for case (ii) (see text for details).

$\tilde{h}(u)$ replacing $h(u)$ in equation (5.9) where

$$\tilde{h}(u) = \begin{cases} f(u,k_3(u)), & u < u^* \\ f(u,k_1(u)), & u > u^*. \end{cases} \tag{5.11}$$

Multiplying by u_x and integrating along orbits from 0 to x, we have the first integral

$$\frac{1}{2}{u_x}^2 + \gamma\Big[H\big(u(x)\big) - H\big(u(0)\big)\Big] = 0 \tag{5.12}$$

where

$$H\big(u(x)\big) \equiv \int_0^{u(x)} h(w)\,\mathrm{d}w \tag{5.13}$$

so that from (5.12) with boundary conditions (5.7)

$$H\big(u(1)\big) = H\big(u(0)\big). \tag{5.14}$$

We can find x from the so-called 'time-map'

$$x = \frac{1}{\sqrt{2\gamma}} \int_{u(0)}^{u(x)} \frac{\mathrm{d}w}{\sqrt{H\big(u(0)\big) - H(w)}} \tag{5.15}$$

where in particular for $x=1$

$$\gamma = \frac{1}{2}\left[\int_{u(0)}^{u(1)} \frac{\mathrm{d}w}{\sqrt{H\big(u(0)\big) - H(w)}}\right]^2 \tag{5.16}$$

and we see that γ parameterises the orbits in the (u,u_x) phase space. In fact it can be shown for a class of kinetic functions of the form we consider here that the time-map (5.16) is a monotonically decreasing function of $u(0)$. This is shown explicitly in a

result by Smoller and Wasserman [124]. Hence we can treat γ and $u(1)$ as functionals of $u(0)$.

There are three possibilities for the solution, depending on the precise form of the kinetics:

1. If $H(u_{min}) < H(u_{max})$ then for every $u(0) \in [u_{min}, u^*]$ there is a γ such that $u(1) \in [u^*, \bar{u}_3]$ exists satisfying (5.14), where $H(\bar{u}_3) = H(u_{min})$. This is the case shown in Figure 5.1(a).
2. If $H(u_{min}) > H(u_{max})$ then for every $u(0) \in [\bar{u}_1, u^*]$ there is a γ such that $u(1) \in [u^*, u_{max}]$ exists satisfying (5.14), where $H(\bar{u}_1) = H(u_{max})$.
3. If we have the symmetric case, where $H(u_{min}) = H(u_{max})$, then for every $u(0) \in [u_{min}, u^*]$ there is a γ such that $u(1) \in [u^*, u_{max}]$ exists satisfying (5.14).

In each case γ is determined by the time-map (5.16). In fact there is an infinite set of γ satisfying (5.16) for particular $u(0)$ and $u(1)$ corresponding to different numbers of cycles of the orbit, which give solutions of different mode.

Put otherwise, for a given γ one can find $u(0)$ and $u(1)$ satisfying the time map (5.16) along with equation (5.14) for a particular number of cycles, where valid solutions have $u(0), u(1) \in [u_{min}, u_{max}]$. Thus γ parameterises the quasi-steady solutions. Now $u(0)$ is a monotonically decreasing function of γ, and so as γ increases the solution may evolve towards a critical point $\gamma = \gamma^c$ at which the solution can no longer be constructed (the solution ceases to exist) and at which point reorganisation to a different mode must occur. For case (i) the critical point will occur at $u(0) = u_{min}$, shown in Figure 5.2(a), while for case (ii) the critical point is reached for $u(0) = \bar{u}_1$ (when $u(1) = u_{max}$), as in Figure 5.2(b) (see also Figure 5.1(b)). Both these conditions are reached simultaneously for case (iii). This analysis is pursued below with a concrete example.

For $\epsilon \neq 0$ these discontinuous solutions do not have sufficient smoothness to satisfy the equations. We treat the equations as a singular perturbation problem and expand about x^* in the stretched variable $\xi = (x - x^*)/\epsilon$ for which we have the inner problem for $U(\xi)$ and $V(\xi)$ describing the transition-layer,

$$0 = U_{\xi\xi} + \epsilon^2 \gamma f(U, V) \tag{5.17}$$

$$0 = V_{\xi\xi} + \gamma g(U, V) \tag{5.18}$$

and so as $|\xi| \to \infty$ we must have $U \to u^*$ and $V_\xi \to 0$ (and thus $V \to k_i(u^*)$ for $i = 1, 3$). Therefore we consider the reduced system where we let $\epsilon \to 0$ and take $U = u^*$ giving

$$0 = V_{\xi\xi} + \gamma g(u^*, V) \tag{5.19}$$

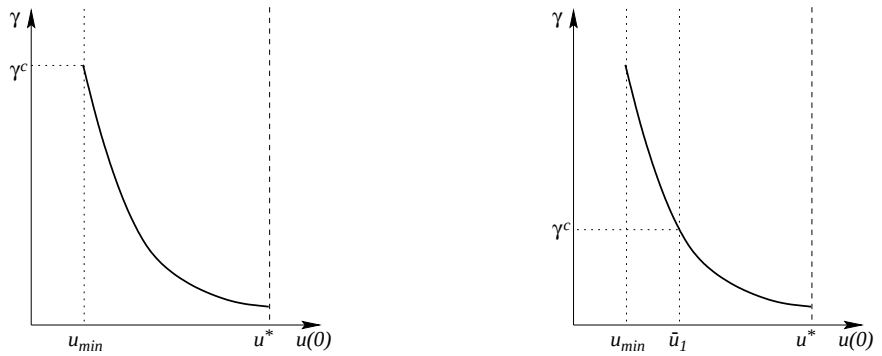

FIGURE 5.2 Evolution towards critical points as γ varies for solutions in the limit as $\epsilon \to 0$. In (a) $H(u_{min}) < H(u_{max})$ so that the solution can no longer be constructed as $u(0)$ decreases through u_{min} with increasing γ (case (i)), and in (b) $H(u_{min}) > H(u_{max})$ for which the solution ceases to exist when increasing γ causes $u(0)$ to decrease below $\bar{u}_1$, when $u(1) = u_{max}$ (case (ii)). When $H(u_{min}) = H(u_{max})$ these points coincide (case (iii)).

and we seek a heteroclinic orbit connecting $V = k_1(u^*)$ and $V = k_3(u^*)$. Multiplying equation (5.19) by V_ξ and integrating over $-\infty < \xi < \infty$ we have

$$G(u^*) \equiv \int_{k_1(u^*)}^{k_3(u^*)} g(u^*, w)\,\mathrm{d}w = 0 \tag{5.20}$$

and from considerations of the sign of g in different regions of the phase space we have for pure kinetics

$$G(u_{min}) > 0 \quad \text{and} \quad G(u_{max}) < 0 \tag{5.21}$$

while, for $g(u, v)$ a decreasing function of u,

$$\frac{\mathrm{d}G}{\mathrm{d}u^*} < 0 \tag{5.22}$$

so that the integral equation uniquely defines u^*, and hence x^*. For cross kinetics the inequalities in (5.21) are reversed and for $g(u, v)$ an increasing function of u then u^* is similarly uniquely determined.

Formally this analysis is equivalent to the leading order calculation in a matched asymptotic expansion. The leading order behaviour is sufficient to establish existence and the basic properties of the large amplitude solutions, including the location of the transition-layer (and dependence on γ). Similarly, periodic patterns may be constructed on the real line. We have said nothing about evolution from initial data or, other than of the outer problem, the stability of the solutions that we construct, and we will generally appeal to the results of numerical simulations for this purpose. However, in the literature various studies have been made of the stability of transition-layer problems. In a similar problem, Fife [39] considers a transition-layer as a travelling

wavefront with zero velocity and shows that a large spatial gradient may evolve from smooth initial data. Furthermore he shows that near the transition region ($x = x^*$) a perturbed wavefront may move back towards x^* under certain conditions.

Next we examine a specific and much simplified model and then investigate the mechanisms for transitions between patterns at the critical points identified above, determining how splitting and insertion are initiated.

5.2 Cubic Autocatalysis Model for Transition-Layer Patterns

Various schemes have been proposed in the literature as models of biochemical reactions with the prerequisites for the Turing bifurcation in a reaction-diffusion system. We consider reaction schemes of polynomial type, and seek to understand the influence of the nonlinearities on transitions between patterns on growing domains. Ermentrout [37] considered the role of quadratic and cubic nonlinearities in reaction terms in the generation of spotted and striped patterns on the two-dimensional domain. Following this example, we will consider the influence of cubic and quadratic nonlinearities in the transitions between patterns. It is informative to expand the kinetic function about the steady state so that the order of different terms is established. For concentration vector $\bar{\mathbf{c}} = \mathbf{c} - \mathbf{c}_s = (\bar{c}_1, \bar{c}_2, \ldots, \bar{c}_n)$ the transformed kinetics are

$$\bar{\mathbf{R}}(\bar{\mathbf{c}}) = \mathbf{R}(\bar{\mathbf{c}} + \mathbf{c}_s) = \mathcal{A}\bar{\mathbf{c}} + \mathcal{N}(\bar{\mathbf{c}}) \tag{5.23}$$

$$= \mathcal{A}\bar{\mathbf{c}} + \mathcal{N}_2(\bar{\mathbf{c}}, \bar{\mathbf{c}}) + \mathcal{N}_3(\bar{\mathbf{c}}, \bar{\mathbf{c}}, \bar{\mathbf{c}}) + \ldots \tag{5.24}$$

and we will assume that $\mathbf{R}$ can be expanded in this way. We note, however, that we no longer expect everywhere positive solutions for $\bar{\mathbf{c}}$, and the physically significant quantities $\mathbf{c}$ are recovered by the addition of the steady state concentrations $\mathbf{c}_s$. In this form the linearised equation contains simply the Jacobian $\mathcal{A}$, which should satisfy the conditions for Turing bifurcation, and the nonlinearities $\mathcal{N}_2$ and $\mathcal{N}_3$ are respectively quadratic and cubic combinations of the $\bar{c}_i$. Hereinafter for notational convenience we drop the over-bars, remembering that solutions may be negative legitimately. We will restrict discussion to include quadratic and cubic nonlinearities only, as these are the highest order terms associated with kinetics such as the Schnakenberg [119], glycolysis [122, 4] and Gray-Scott [45] models. The system may be further simplified by supposing that the nonlinear terms are in v and appear only in the activator equation (in $g(u, v)$). Then considerations in the phase plane on the orientation of the nullcline curve dictate that the cubic term in the kinetics must be negative (for both pure and cross kinetics). Below it is shown numerically that this kinetic model can give rise to Turing bifurcation to finite amplitude pattern, and that a sequence of patterns may form on the growing domain as normal. We will consider reaction terms which consist solely of odd powers of the dependent variables such that the reaction-diffusion system is invariant under the parity transformation

$$(u, v) \to (-u, -v) \tag{5.25}$$

and investigate the effect on pattern formation of quadratic perturbations which break the symmetry.

We can choose the linear part of the reaction term to admit the Turing bifurcation (although this is not required for the existence of large amplitude patterns of the form we have described) and specify the relative polarities of the spatial profiles for activator and inhibitor species according to the signs of the entries in the matrix $\mathcal{A}$. Initially we choose a pure kinetic system, in which the Fourier modes destabilising the spatially homogeneous state are spatially in phase for the activator and inhibitor. The nonlinear kinetics are given by f and g where

$$f(u,v) = -\sigma u + v \tag{5.26}$$

$$g(u,v) = -u + \mu v + \delta v^2 - v^3 \tag{5.27}$$

where the positive constants σ and μ are such that the linearised system,

$$\mathcal{A} = \begin{bmatrix} -\sigma & 1 \\ -1 & \mu \end{bmatrix}. \tag{5.28}$$

satisfies the conditions for DDI. The effect of quadratic terms on the behaviour of a system which is predominantly cubic is examined by introducing a small quadratic contribution, $|\delta| \ll 1$. In chemically oriented discussions of cubic autocatalysis the cubic term is usually given by uv^2. This form generates the same qualitative behaviour, while begin less easily studied analytically, and so to examine the role of the nonlinearities we proceed with the cubic in v.

In practice, even with this simple form, the nonlinearities in the equations are such that construction of the transition-layer solutions is a nontrivial exercise. The inner equations are easily integrated, but the $k_i(u)$ are the roots of a cubic and for the outer equations a simple closed form solution cannot be found. However, the essential features of the kinetic system are well approximated by a piece-wise linear version of the reaction term.

5.2.1 Piece-wise Linear Approximation. The use of a piece-wise linear approximation to a nonlinear function is a means of rendering a nonlinear system analytically tractable (see for example Rinzel and Keller [117] and Lane *et al.* [68]). We introduce a piece-wise linear scheme which retains the qualitative features of the nullclines of the nonlinear system (5.26)–(5.27), defined so that for $\delta = 0$ the turning points in the v-nullcline coincide with those for the full nonlinear problem. If we insist that the steady state of the kinetics is at the origin (so that the linearised system is simply the linear part of the kinetics) then it is desirable that the nullcline be continuous here. Therefore we approximate the nullcline by three linear regions. We will consider the effect of introducing a non-zero quadratic contribution by removing the symmetry of the nullcline, as will be shown in detail later. In general the gradient of the nullcline can be different in each of the linear regions, but to preserve the symmetry we

take equal gradients modulo their sign. For a pure kinetic system (5.26)–(5.27) the piece-wise linear reaction term is

$$f(u,v) = -\sigma u + v \tag{5.29}$$

$$g(u,v) = g_i = \begin{cases} g_1 \\ g_2 \\ g_3 \end{cases} = \begin{cases} -u - \eta(v + 2\theta_1), & v < -\theta_1 \\ -u + \eta v, & -\theta_1 \leq v \leq \theta_3 \\ -u - \eta(v - 2\theta_3), & v > \theta_3 \end{cases} \tag{5.30}$$

where $i = 1, 2, 3$ define the three branches of the v-nullcline, dividing (u, v) space into 3 regions at the turning points where $v = -\theta_1$ and $v = \theta_3$ respectively, where θ_1 and θ_3 are positive constants. We will use subscripts to refer to these three regions. The piece-wise linear kinetics are such that the reaction term is continuous at $v = -\theta_1$ and $v = \theta_3$ for all u, and exhibit a unique fixed point (at the origin) for $\eta\sigma < 1$. In order that the turning points for the v-nullcline with $\delta = 0$ are at the same locations as for the nonlinear kinetics, we modify one of the parameters in the linearised equations, defining the positive constant

$$\eta = \frac{2\mu}{3}. \tag{5.31}$$

This does not qualitatively change the behaviour of the equations. Furthermore, we approximate the turning points for $\delta \neq 0$ by

$$\theta_{1,3} = \frac{1}{3}\left(\sqrt{3\mu + \delta^2} \mp \delta\right) \tag{5.32}$$

which takes the appropriate values for v but not, therefore, for u.

We have chosen parameters such that the Turing bifurcation is still admitted in the linearised system with

$$\mathcal{A}' = \begin{bmatrix} -\sigma & 1 \\ -1 & \eta \end{bmatrix}. \tag{5.33}$$

Activator solutions on the slow uniformly growing domain for the full nonlinear kinetics (5.26)–(5.27) and for the piece-wise linear scheme (5.29)–(5.30) are compared in Figure 5.3. All three possible sequence types are illustrated: frequency-doubling by peak splitting in (a) and (b) and by peak insertion for (e) and (f), while (c) and (d) show frequency-tripling, where peak splitting and insertion occur simultaneously. The frequency-doubling sequences are recovered by the addition of small quadratic-like perturbations to the kinetics, the sign of which determines the method of transition between quasi-steady patterns. In these cases the parity symmetry is broken by moving one turning point for the v-nullcline relative to the other, according to equation (5.32). In each case the nonlinear and piece-wise linear kinetics are shown to give qualitatively similar results.

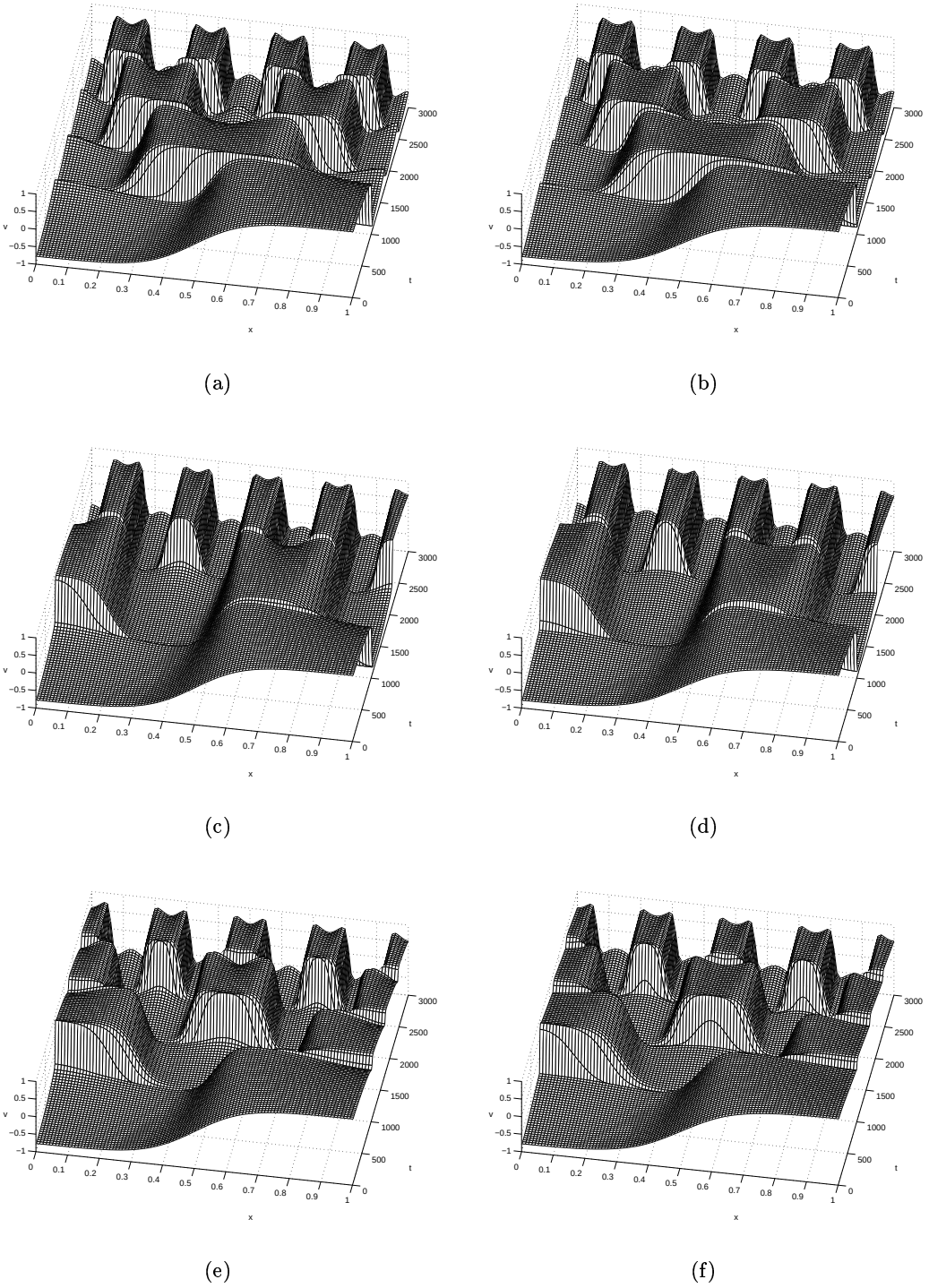

FIGURE 5.3 Comparison of activator pattern sequences generated with nonlinear kinetics (5.26)–(5.27), shown in the left-hand figures, and piece-wise linear kinetics (5.29-5.30), shown on the right-hand, with $\sigma = 1.0$ and $\mu = 0.8$ (so that $\eta = 2\mu/3 = 0.533$). For (a) and (b) $\delta = -0.01$ giving frequency-doubling by peak splitting, while for (e) and (f) $\delta = 0.01$ and the sequence is generated by peak insertion. For (c) and (d) $\delta = 0$ (the nonlinearities are cubic) and the sequence generated exhibits frequency-tripling.

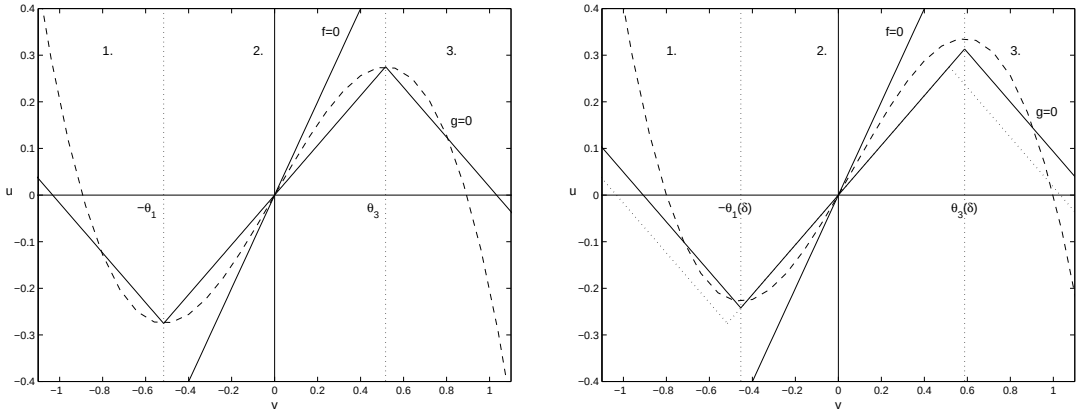

(a) (b)

FIGURE 5.4 Nullclines for piece-wise linear kinetics (5.34)–(5.35). Superimposed is the v-nullcline for the nonlinear cubic autocatalysis system (5.27) (dashed line), with $\sigma = 1.0$ and $\mu = 0.8$ ($\eta = 0.533$). In (a) we plot the symmetric case ($\delta = 0$) and in (b) we introduce a quadratic perturbation ($\delta = 0.2$) (the symmetric case is shown by the dotted line).

Nullclines for this system, given by

$$f(u,v) = 0, \qquad u = \frac{1}{\sigma} v \tag{5.34}$$

$$g(u,v) = 0, \qquad u = \begin{cases} -\eta(v + 2\theta_1), & v < -\theta_1 \\ \eta v, & -\theta_1 \leq v \leq \theta_3 \\ -\eta(v - 2\theta_3), & v > \theta_3 \end{cases} \tag{5.35}$$

are plotted in Figure 5.4, where we have superimposed the v-nullcline for the full nonlinear system (5.27).

The piece-wise linear reaction-diffusion system may, naturally, be solved exactly in each of the three regions of the reaction term, and the undetermined constants eliminated by matching solution segments together appropriately. However, such an undertaking is algebraically challenging, sufficiently so to obscure the insights to be gained from the approximation. Indeed we quickly find that the solution cannot be expressed in closed form. Therefore we pursue an asymptotic approximation where we will consider only the leading order terms in an expansion in ϵ.

5.3 Matched Asymptotic Analysis for the Piece-wise Linear System

Initially we will consider a solution with a single transition-layer on the domain (corresponding to a pattern of lowest mode) at

$$x = x^* \in [0,1]. \tag{5.36}$$

From our discussion of pattern symmetries in Chapter 2 we recognise this as the basic building block for steady state patterns of higher mode. Away from the transition-layer itself, solutions lie on the nullcline $g = 0$ in regions $i = 1$ and $i = 3$, the former corresponding to $v < 0$ and the latter to $v > 0$. Therefore we take $v = k_1(u)$ near $x = 0$, so that $h(u)$ is defined as in section 5.1, and the transition-layer is a step increase in v (corresponding to a pattern of negative polarity). Formally we assume an expansion in powers of ϵ

$$u(x,\epsilon) \sim \sum_{j=0}^{\infty} \epsilon^j u^{(j)}(x), \qquad v(x,\epsilon) \sim \sum_{j=0}^{\infty} \epsilon^j v^{(j)}(x). \tag{5.37}$$

For the leading order problem we will drop the superscripts. Substituting the expansions into the steady state equations and collecting leading order terms we recover equation (5.9), which determines the variation of u across the domain, where for region 1,

$$u_{xx} - \gamma\lambda^2 u = 2\gamma\theta_1, \qquad u_x(0) = 0 \tag{5.38}$$

with solution

$$u_1(x) = a_1 \cosh(\lambda\sqrt{\gamma}x) - \frac{2\theta_1}{\lambda^2} \tag{5.39}$$

where

$$\lambda \equiv \sqrt{\sigma + \frac{1}{\eta}}. \tag{5.40}$$

Similarly in region $i = 3$ of the phase plane

$$u_3(x) = a_3 \cosh\left(\lambda\sqrt{\gamma}\,(1-x)\right) + \frac{2\theta_3}{\lambda^2} \tag{5.41}$$

which satisfies the zero flux condition at $x = 1$. These equations also determine the activator profiles in the outer regime through the relations $v_i(x) = k_i\big(u_i(x)\big)$,

$$v_1(x) = -\frac{a_1}{\eta}\cosh(\lambda\sqrt{\gamma}x) - \frac{2\sigma\theta_1}{\lambda^2} \tag{5.42}$$

$$v_3(x) = -\frac{a_3}{\eta}\cosh\left(\lambda\sqrt{\gamma}\,(1-x)\right) + \frac{2\sigma\theta_3}{\lambda^2}. \tag{5.43}$$

Taking as the inner variable $\xi = (x - x^*)/\epsilon$, the solution, (U, V), in the vicinity of the transition-layer is written as a power series in ϵ

$$U(\xi,\epsilon) \sim \sum_{j=0}^{\infty} \epsilon^j U^{(j)}(\xi), \qquad V(\xi,\epsilon) \sim \sum_{j=0}^{\infty} \epsilon^j V^{(j)}(\xi) \tag{5.44}$$

(again, in the leading order calculation we will omit the superscript). The leading order term in U is determined by equation (5.3). Linear dependence on ξ will not match with the outer solution, as calculated above, and so in the inner region we

assume

$$U = u^*. \tag{5.45}$$

This constant is determined by the integral (5.20) which we can evaluate easily enough, giving

$$u^* = \frac{1}{2}\eta\left(\theta_3 - \theta_1\right). \tag{5.46}$$

Thus we find that the value of u in the transition-layer does not depend on γ.

Construction of the inner solution for V is complicated by the fact that we must piece together solutions for regions $i = 1, 2$ and 3, requiring continuity of the solution where the kinetics change abruptly for $V = -\theta_1$ at a spatial location we denote as ξ_{12} and again where $V = \theta_3$, at the point ξ_{23}. In region $i = 1$, for which $g = g_1(u^*, V)$, we have

$$V_{\xi\xi} - \gamma\eta V = \frac{1}{2}\gamma\eta\left(3\theta_1 + \theta_3\right) \tag{5.47}$$

and we take the solution which decays as $\xi \to -\infty$

$$V_1(\xi) = b_1 \exp\left(\sqrt{\gamma\eta}\xi\right) - \frac{1}{2}\left(3\theta_1 + \theta_3\right). \tag{5.48}$$

Similarly in region 3 we find

$$V_3(\xi) = b_3 \exp\left(-\sqrt{\gamma\eta}\xi\right) + \frac{1}{2}\left(\theta_1 + 3\theta_3\right) \tag{5.49}$$

which decays as $\xi \to \infty$. In region $i = 2$ the leading order term in V satisfies

$$V_{\xi\xi} + \gamma\eta V = \frac{1}{2}\gamma\eta\left(\theta_3 - \theta_1\right) \tag{5.50}$$

for which

$$V_2(\xi) = b_2 \sin\left(\sqrt{\gamma\eta}\xi + \beta\right) + \frac{1}{2}\left(\theta_3 - \theta_1\right). \tag{5.51}$$

For continuity we require

$$V_1(\xi_{12}) = V_2(\xi_{12}) = -\theta_1 \tag{5.52}$$

$$V_2(\xi_{23}) = V_3(\xi_{23}) = \ \theta_3 \tag{5.53}$$

$$\left[V_1\right]_\xi(\xi_{12}) = \left[V_2\right]_\xi(\xi_{12}), \qquad \left[V_2\right]_\xi(\xi_{23}) = \left[V_3\right]_\xi(\xi_{23}) \tag{5.54}$$

and we seek to determine the six unknowns b_i, for $i = 1, 2, 3$, ξ_{12}, ξ_{23} and β. However, solving these equations we find

$$\xi_{12} = \frac{1}{\sqrt{\gamma\eta}}\left(-\frac{\pi}{4} - \beta\right), \qquad \xi_{23} = \frac{1}{\sqrt{\gamma\eta}}\left(\frac{\pi}{4} - \beta\right) \tag{5.55}$$

so that the intersection locations are known up to undetermined phase β. This means that in the leading order calculation we cannot determine the points ξ_{12} and ξ_{23} *within*

the transition-layer.[2] However, for $\beta \sim \mathcal{O}(1)$ this introduces only $\mathcal{O}(\epsilon)$ error in the location of the transition layer $x = x^*$. Taking $\beta = 0$, which is reasonable in particular for $\theta_1 = \theta_3$ where the transition is symmetrical about $\xi = 0$, we find on substituting $U = u^*$

$$V_1(\xi) = \frac{1}{2}(\theta_1 + \theta_3)\exp\left[\sqrt{\gamma\eta}\,\xi + \frac{\pi}{4}\right] - \frac{1}{2}(3\theta_1 + \theta_3) \tag{5.56}$$

$$V_2(\xi) = \frac{1}{\sqrt{2}}(\theta_1 + \theta_3)\sin\left[\sqrt{\gamma\eta}\,\xi\right] + \frac{1}{2}(\theta_3 - \theta_1) \tag{5.57}$$

$$V_3(\xi) = -\frac{1}{2}(\theta_1 + \theta_3)\exp\left[-\sqrt{\gamma\eta}\,\xi + \frac{\pi}{4}\right] + \frac{1}{2}(\theta_1 + 3\theta_3) \tag{5.58}$$

and the inner solution is determined up to the unknown position x^*, which may vary with γ.

To find the constants a_1 and a_3 we match the leading order inner and outer solutions. Writing the outer solution for u in the inner variable, $x = \epsilon\xi + x^*$, and letting $\epsilon \to 0$ we find

$$a_1(x^*) = \frac{1}{\cosh(\lambda\sqrt{\gamma}x^*)}\left(u^* + \frac{2\theta_1}{\lambda^2}\right) \tag{5.59}$$

$$a_3(x^*) = \frac{1}{\cosh\left(\lambda\sqrt{\gamma}\,(1 - x^*)\right)}\left(u^* - \frac{2\theta_3}{\lambda^2}\right) \tag{5.60}$$

and matching in v follows automatically. Thus we obtain composite solutions, noting explicitly the dependence on γ (and hence dimensional domain length)

$$u(x) \sim a_1(\gamma)\cosh\left(\lambda\sqrt{\gamma}x\right) - \frac{2\theta_1}{\lambda^2}, \qquad 0 \le x < x^*(\gamma) \tag{5.61}$$

$$\sim a_3(\gamma)\cosh\left(\lambda\sqrt{\gamma}\,(1 - x)\right) + \frac{2\theta_3}{\lambda^2}, \qquad x^*(\gamma) \le x \le 1 \tag{5.62}$$

and

$$v(x) \sim -\frac{a_1(\gamma)}{\eta}\cosh\left(\lambda\sqrt{\gamma}x\right) + \frac{1}{2}(\theta_1 + \theta_3)\exp\left[\frac{\pi}{4} + \sqrt{\gamma\eta}\left(\frac{x - x^*(\gamma)}{\epsilon}\right)\right] - \frac{2\sigma\theta_1}{\lambda^2}, \qquad 0 \le x < x_{12}(\gamma) \tag{5.63}$$

$$\sim -\frac{a_1(\gamma)}{\eta}\cosh\left(\lambda\sqrt{\gamma}x\right) + (\theta_1 + \theta_3)\left[\frac{1}{\sqrt{2}}\sin\left[\sqrt{\gamma\eta}\left(\frac{x - x^*(\gamma)}{\epsilon}\right)\right] + 1\right] - \frac{2\sigma\theta_1}{\lambda^2}, \quad x_{12}(\gamma) \le x < x^*(\gamma) \tag{5.64}$$

[2] We could simplify the analysis somewhat, at the expense of introducing an error in the inner region which may not be $\mathcal{O}(\epsilon)$, by neglecting the inner solution in region 2 completely and matching solutions in regions 1 and 3. Then continuity at $\xi = 0$ determines the constants b_1 and b_3.

$$\sim -\frac{a_3(\gamma)}{\eta}\cosh\left(\lambda\sqrt{\gamma}(1-x)\right) + (\theta_1+\theta_3)\left[\frac{1}{\sqrt{2}}\sin\left[\sqrt{\gamma\eta}\left(\frac{x-x^*(\gamma)}{\epsilon}\right)\right]-1\right]+\frac{2\sigma\theta_3}{\lambda^2}, \quad x^*(\gamma)\le x < x_{23}(\gamma) \tag{5.65}$$

$$\sim -\frac{a_3(\gamma)}{\eta}\cosh\left(\lambda\sqrt{\gamma}(1-x)\right) - \frac{1}{2}(\theta_1+\theta_3)\exp\left[\frac{\pi}{4}-\sqrt{\gamma\eta}\left(\frac{x-x^*(\gamma)}{\epsilon}\right)\right]+\frac{2\sigma\theta_3}{\lambda^2}, \qquad x_{23}(\gamma)\le x\le 1 \tag{5.66}$$

where the points x_{12} and x_{23} correspond to the locations at which the kinetic term changes between regions 1 and 2, and 2 and 3 respectively, and are given by

$$x_{12}(\gamma) = x^*(\gamma) - \frac{\epsilon\pi}{4\sqrt{\gamma\eta}}, \qquad x_{23}(\gamma) = x^*(\gamma) + \frac{\epsilon\pi}{4\sqrt{\gamma\eta}}. \tag{5.67}$$

The final condition required to determine the location of the transition-layer comes from integrating equation (5.9). As $u(x)$ is continuous across the domain

$$\int_0^1 h(u)\,\mathrm{d}x = 0 \tag{5.68}$$

obtains for $h(u)$ defined as in equation (5.10). Evaluating to leading order gives

$$a_1\sinh\left(\lambda\sqrt{\gamma}x^*\right) = -a_3\sinh\left(\lambda\sqrt{\gamma}\left(1-x^*\right)\right) \tag{5.69}$$

which states, consistently, that the gradient of u is continuous across the transition-layer. Eliminating constants a_1 and a_3 using (5.59) and (5.60) we have for $x^*(\gamma)$

$$\bar{\theta}_1\tanh(\lambda\sqrt{\gamma}x^*) = \bar{\theta}_3\tanh(\lambda\sqrt{\gamma}(1-x^*)) \tag{5.70}$$

where we have defined

$$\bar{\theta}_1 \equiv \frac{2\theta_1}{\lambda^2}+u^*, \qquad \bar{\theta}_3 \equiv \frac{2\theta_3}{\lambda^2}-u^* \tag{5.71}$$

which are independent of γ. Clearly for the symmetric case, $\theta_1=\theta_3$, $x^*=1/2$ and the transition-layer does not move with γ (and hence changing domain length). For the general case we solve by writing $x^*=(\ln z)/2\lambda\sqrt{\gamma}$ and expanding (5.70) to obtain the quadratic in z

$$\left(\bar{\theta}_1+\bar{\theta}_3\right)z^2+\left(\bar{\theta}_1-\bar{\theta}_3\right)\left(\exp\left(2\lambda\sqrt{\gamma}\right)-1\right)z-\exp\left(2\lambda\sqrt{\gamma}\right)\left(\bar{\theta}_1+\bar{\theta}_3\right)=0 \tag{5.72}$$

for which we take the positive solution $z_+(\gamma)$. In order that $x^*(\gamma)\in[0,1]$ we must have $1\le z_+(\gamma)\le\exp\left(2\lambda\sqrt{\gamma}\right)$, for which we require

$$\left|\frac{\bar{\theta}_3-\bar{\theta}_1}{\bar{\theta}_3+\bar{\theta}_1}\right|\le 1 \tag{5.73}$$

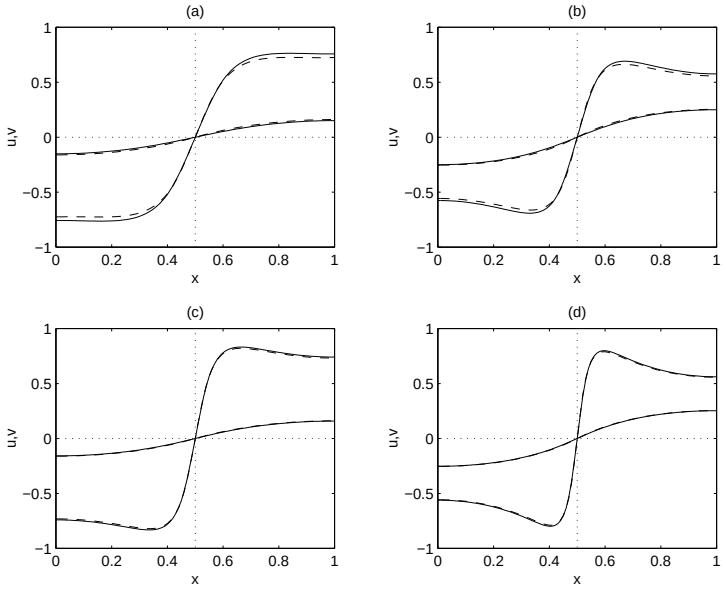

FIGURE 5.5 Numerical solution (solid) and asymptotic approximation (dashed) for piece-wise linear kinetics with $\sigma = 1.0$, $\mu = 0.8$ ($\eta = 0.533$) and $\delta = 0$ (the symmetric case) on the fixed domain. Activator solutions have larger amplitude than inhibitor solutions (both are shown). Figures (a) and (b) have $\epsilon = 0.1$ while (c) and (d) have $\epsilon = 0.05$. For the left-hand figures $\gamma = 2.0$; for the right-hand plots $\gamma = 6.0$. The analytical approximation improves as ϵ is decreased.

and this inequality holds always for $\theta_1, \theta_3 \geq 0$ along with the condition for monostability, $\eta\sigma < 1$. Also, it follows that when $\theta_3 \geq \theta_1$, $x^* \geq 1/2$, and similarly the reverse is also true.

This completes the construction of the solution to the steady state problem. In Figures 5.5 and 5.6 we plot steady state numerical solutions of equations (5.5)–(5.6) with piece-wise linear kinetics (5.29)–(5.30) and the analytical solutions given in equations (5.61)–(5.66). For the analytical solutions the location of the transition-layer $x^*(\gamma)$ is calculated as above, and we compare the solutions for two values of the small parameter ϵ. In Figure 5.5 we take $\delta = 0$ such that $\theta_1 = \theta_3$ and the location of the transition-layer is shown to be independent of γ, while comparing left- to right-hand plots we see that the transition becomes narrower (and increasingly steep) for larger γ. When $\delta > 0$ then $\theta_3 > \theta_1$ and the transition-layer moves to the right for increasing values of γ, as shown in Figure 5.6. These figures suggest that the analytical solution that we have constructed converges to the true solution as ϵ is decreased. In Figure 5.7 we plot the L^2 error for each of these δ and γ parameter combinations.

Using the symmetry argument for steady state solutions, presented in Chapter 2, patterns of higher spatial mode may be constructed by piecing together sections corresponding to the lowest mode pattern, appropriately reflected and scaled. Alternatively we can interpret this result to identify each half-wavelength section of a pattern of higher mode (with zero flux boundaries) with the lowest mode pattern (with γ scaled

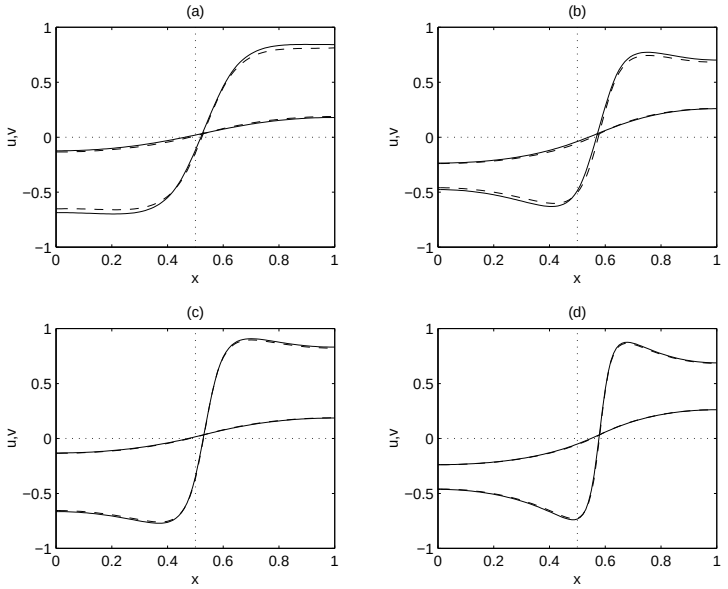

FIGURE 5.6 Numerical solution (solid) and asymptotic approximation (dashed) for piece-wise linear kinetics with $\delta = 0.2$ and other details as for Figure 5.5. In (a) and (b) we have $\epsilon = 0.1$ while for (c) and (d) $\epsilon = 0.05$. For the left-hand figures $\gamma = 2.0$; for the right-hand plots $\gamma = 5.0$.

appropriately). This may also be understood by considering the time-map (5.16) where patterns of higher mode correspond to multiple circuits of the orbit in the (u, u_x) plane for the lowest-mode pattern, so that a solution consisting of m circuits of the same orbit exists when γ is scaled by a factor m^2. Thus for the time-independent problem each half-wavelength section will vary with γ in the same manner. For slow uniform domain growth, the evolving PDE solution in the quasi-steady regime remains in the vicinity of these steady state solutions. Thus we may seek to understand the behaviour of higher pattern modes when γ increases with time by considering only the simplest pattern on the domain.

5.4 Transitions Between Patterns on the Growing Domain

We have constructed an approximate solution to the time-independent problem which is valid for γ less than a critical value, γ^c, which we calculate below. For γ greater than this value the steady solution of lowest pattern mode no longer exists. On the slowly growing domain, ρ small, this analytical solution approximates the quasi-steady pattern and is valid up to the point at which a pattern of higher spatial frequency is established for the PDE. The limiting feature for the construction of the analytical solution, as γ increases through the critical value, determines the mechanisms of breakdown for the full reaction-diffusion system. Furthermore, once the critical value γ^c is established for the lowest mode, the symmetry analysis tells us the values for breakdown for higher modes m through the scaling by the factor m^2.

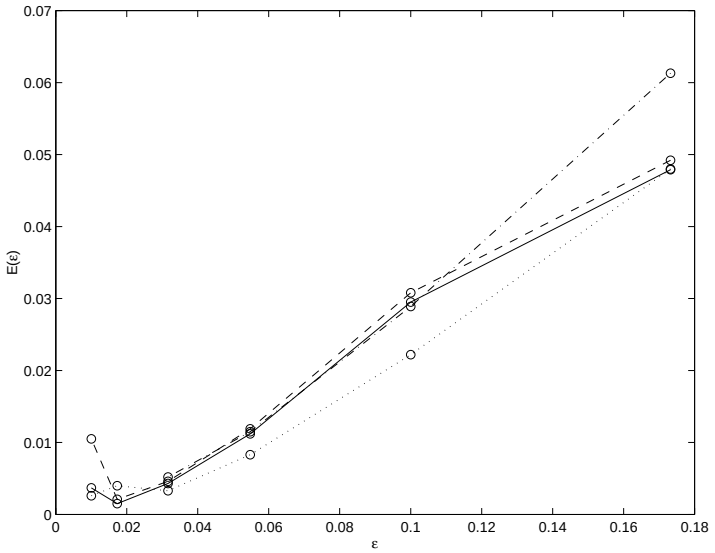

FIGURE 5.7 L^2 error, $E(\epsilon)$, for the analytical expressions for the activator solution v compared to numerical solutions with $\gamma = 2.0$, $\delta = 0.0$ (solid), $\gamma = 5.0$, $\delta = 0.0$ (dotted), $\gamma = 2.0$, $\delta = 0.2$ (dashed) and $\gamma = 5.0$, $\delta = 0.2$ (dot-dashed). Before calculating $E(\epsilon)$ it was verified that the numerical solutions were in the steady state.

5.4.1 Peak Splitting and Insertion. In the steady state the outer solution is constrained to lie on the v-nullcline. For slow uniform domain growth the quasi-steady solution evolves until this condition can no longer be satisfied. As γ increases the solutions are limited by the turning points of the v-nullcline,

$$u_{min} = -\eta\theta_1, \qquad u_{max} = \eta\theta_3. \tag{5.74}$$

For the lowest pattern mode $u(x)$ is monotonically increasing and the maximum and minimum occur at the domain boundaries. As γ is increased, one of these boundary values increases through one of the turning points. Activator peak splitting or peak insertion ensues, according to which of the points u_{min} or u_{max} is reached first. In the symmetric case, where $\theta_1 = \theta_3$, both points are reached for the same value of γ and simultaneous splitting and insertion follows, as demonstrated in the numerical simulations shown in Figures 5.3(c) and 5.3(d), described as frequency-tripling. For particular parameter sets we can use the values of u at the boundaries to predict the critical γ at which the transition between pattern modes occurs, and by which mechanism.

At the domain boundaries, from equations (5.61)–(5.62) we have $u(0)$ and $u(1)$ as functions of γ

$$u(0) = a_1(\gamma) - \frac{2\theta_1}{\lambda^2}, \qquad u(1) = a_3(\gamma) + \frac{2\theta_3}{\lambda^2}. \tag{5.75}$$

Now if $u(0) = u_{min}$ at $\gamma = \gamma_1^c$ then substituting for $a_1(\gamma)$ in the first of (5.75) we find

$$\lambda\sqrt{\gamma}x^*(\gamma) = \cosh^{-1}\left[\frac{\lambda^2\bar{\theta}_1}{2\theta_1 - \eta\lambda^2\theta_1}\right] \equiv \phi_1 \tag{5.76}$$

where ϕ_1 is independent of γ. Substituting this into equation (5.72) with $z = z_1 = \exp 2\phi_1$, after some algebra we find

$$\gamma_1^c = \left[\frac{1}{2\lambda}\ln\left(\frac{(\bar{\theta}_1 + \bar{\theta}_3)z_1^2 - (\bar{\theta}_1 - \bar{\theta}_3)z_1}{(\bar{\theta}_1 + \bar{\theta}_3) - (\bar{\theta}_1 - \bar{\theta}_3)z_1}\right)\right]^2. \tag{5.77}$$

Similarly, substituting into the second equation of (5.75),

$$\lambda\sqrt{\gamma}x^*(\gamma) = \cosh^{-1}\left[\frac{\lambda^2\bar{\theta}_3}{2\theta_3 - \eta\lambda^2\theta_3}\right] \equiv \phi_3 \tag{5.78}$$

where ϕ_3 is independent of γ, and we find that $u(1) = u_{max}$ at $\gamma = \gamma_3^c$ where

$$\gamma_3^c = \left[\frac{1}{2\lambda}\ln\left(\frac{(\bar{\theta}_1 + \bar{\theta}_3)z_3^2 + (\bar{\theta}_1 - \bar{\theta}_3)z_3}{(\bar{\theta}_1 + \bar{\theta}_3) + (\bar{\theta}_1 - \bar{\theta}_3)z_3}\right)\right]^2 \tag{5.79}$$

for $z_3 = \exp 2\phi_3$. From the discussion of the time-map (5.16) in section 5.1, if γ is a monotonically decreasing function of $u(0)$ (see Figure 5.2),

$$\frac{\mathrm{d}u(0)}{\mathrm{d}\gamma} < 0, \tag{5.80}$$

then the quasi-steady approximation breaks down as $u(0)$ decreases through u_{min} where the solution branch disappears. Then locally $g < 0$ and so from equation (5.8), which determines the dynamics in the outer part of the solution, we have $v_t < 0$ (in the fast timescale). For u below u_{min}, branch 3 of the nullcline $g = 0$ is attracting for this dynamical system and the v-solution relaxes to this branch on the fast timescale, giving a sudden growth of activator at the boundary (where there had been a minimum in the solution profile). This is pattern transition via insertion of a new activator peak (see the dashed arrow (i) in Figure 5.1(b)). By a similar argument on the time-map (5.16), γ may be shown to be an monotonic increasing function of $u(1)$ (see [124]) so that

$$\frac{\mathrm{d}u(1)}{\mathrm{d}\gamma} > 0 \tag{5.81}$$

and the solution ceases to exist if $u(1)$ increases through u_{max} before u_{min} is reached. Here $g > 0$ and $v_t > 0$ and so the v-solution relaxes to branch 1 of the nullcline on the fast timescale giving a sudden collapse at the activator peak, producing pattern change by activator peak splitting (see the dashed arrow (ii) in Figure 5.1(b)). When the boundary values pass through these critical points at the same value of γ, due to the symmetry of the kinetics, both splitting and insertion occur simultaneously.

These critical points are functions of the kinetic parameters and in particular θ_1 and θ_3. In Figure 5.8 we plot the analytical predictions as functions of δ, such that θ_1 and θ_3 vary according to equation (5.32), where $\theta_1 < \theta_3$ for $\delta > 0$ and correspondingly

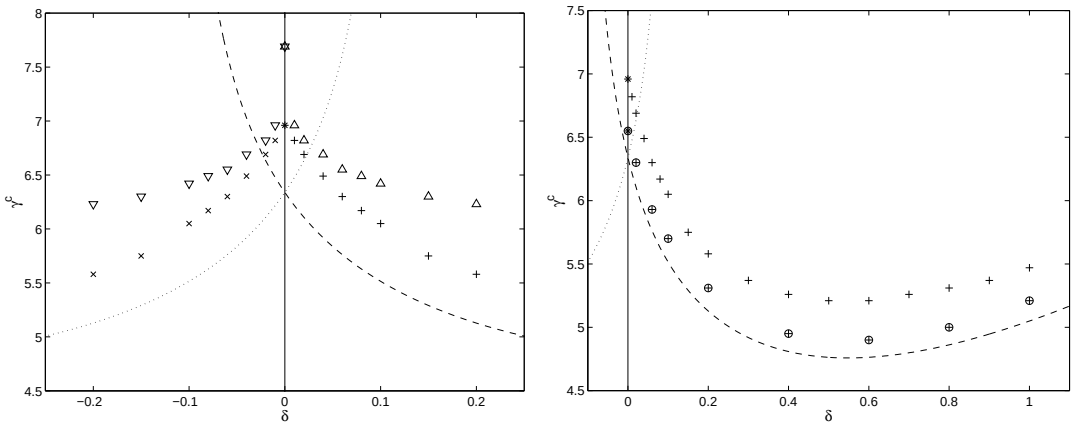

(a) (b)

FIGURE 5.8 Figures showing the analytical prediction of critical γ for pattern transitions by peak splitting, γ_3^c, (dotted) and insertion, γ_1^c, (dashed) given in equations (5.79) and (5.77) respectively, as functions of δ. Other kinetic parameters are as in Figure 5.5. In (a) points for splitting (marked $\times$) and insertion (+) and simultaneous splitting and insertion (marked $*$) are shown for numerical solutions with piece-wise linear kinetics on the growing domain with $\rho = 0.0001$. The darts indicate points for transitions in the full nonlinear system via splitting (marked $\triangledown$) and insertion ($\triangle$) (with both marks for simultaneous splitting and insertion). For both sets of data we have $\epsilon = 0.1$. In (b) we plot points for the onset of activator peak insertion for numerical solutions with the piece-wise linear scheme for $\epsilon = 0.1$ ($\times$) and $\epsilon = 0.05$ (circled symbols), showing convergence to the analytical predictions as $\epsilon \to 0$. There is an inherent error introduced in judging when the onset of the transition occurs for the numerical simulations. However, for small ρ the onset is very sudden, and we have taken a sufficiently small timestep for the numerical integration that γ^c can be identified to within ± 0.05.

we have insertion for $\delta > 0$ (dashed line) and activator peak splitting for $\delta < 0$ (dotted line). Both curves, $\gamma_1^c(\delta)$ and $\gamma_3^c(\delta)$, extend on either side of $\delta = 0$ and we expect to observe the behaviour which occurs at lower γ.[3] In Figure 5.8(a) we plot points for splitting and insertion obtained from numerical simulations for both piece-wise linear kinetics (crosses) and for the full nonlinear system (darts) on the slowly growing domain, showing qualitatively similar behaviour for small δ. Previously, in Figure 5.3, it was shown that the evolution of pattern sequences on the growing domain is similar for the nonlinear scheme and its piece-wise linear approximation, and this is reinforced here in the transition behaviour at the critical γ, from which we infer that the piece-wise linear approximation is a reasonable one. In Figure 5.8(b) we plot points obtained from numerical simulations for the onset of activator peak insertion for the piece-wise linear scheme for two values of ϵ, showing that the numerically derived values approach the analytical prediction as ϵ is decreased. For the growing domain

[3] In fact the curves do not extend very far on opposite sides of $\delta = 0$ as the curves tend to their asymptotes where the denominators in equations (5.77) and (5.79) go to zero.

we expect that there is also a contribution to the error from the rate of slow domain growth, and that as ϵ is decreased the numerical γ^c for onset of the transition will approach the analytically predicted value as $\rho \to 0$.

5.4.2 Spatial Frequency-Tripling. We have described a new phenomenon, spatial frequency-tripling, which is realised on the slowly growing domain when the reaction-diffusion equation is symmetric under the transformation $(u, v) \to (-u, -v)$.[4] We have shown previously that steady state solutions with three times the spatial frequency may be constructed from lower-mode solutions of the time-independent problem. However, it is also useful to show that the symmetry argument in the full PDE system, outlined in section 4.2.1 for spatial frequency-doubling, also accommodates this sequence. It is straightforward to show that the full reaction-diffusion equation (4.22) is invariant under the transformation $(x, \gamma) \to (\bar{p}_3(x), \gamma/9)$ where the map

$$\bar{p}_3(x) = \begin{cases} 1 - 3x, & 0 \leq x < \frac{1}{3} \\ 3x - 1, & \frac{1}{3} \leq x < \frac{2}{3} \\ 3(1 - x), & \frac{2}{3} \leq x \leq 1 \end{cases} \tag{5.82}$$

corresponds to frequency-tripling, and the factor of $\gamma/9$ for the transformation corresponds to the dimensional domain length changing by a factor of three. The same arguments may then be applied as previously, such that if the solution $c(x, 9\gamma^*)$ matches the construction at three times the spatial frequency, $q_3(x, \gamma^*) \equiv c(\bar{p}_3(x), \gamma^*)$, for some $\gamma = \gamma^*$ (rather than matching a construction with twice the spatial frequency at $4\gamma^*$) then the frequency-tripling sequence should ensue, subject to the same proviso concerning stability, which again we must conjecture from numerical results.

5.5 Discussion

Considering a piece-wise linear model of reaction and diffusion generating patterns of transition-layer type, we have been able to determine the method of pattern reorganisation on the growing domain and predict the onset of transitions by considering the existence of solutions to the associated steady-state problem. Thus far we have not considered the stability of these solutions (see the work of Kerner *et al.* for a lengthy discussion [62]). The heterogeneous solutions which we have constructed disappear when still at large amplitude (rather than with amplitude decaying to zero as γ increases through a bifurcation point of the homogeneous steady state). Furthermore, numerical simulations for the growing domain problem have shown that the quasi-steady solutions are stable as γ increases up to the value, γ^c, where the steady state solution branch ceases to exist, at which point transitions to higher pattern mode take place. This suggests that the branch of steady state heterogeneous solutions that

[4] It is interesting to note that the symmetry required for frequency-tripling is the same as that required for preferential selection of stripes over spots in two-dimensional pattern formation in reaction-diffusion systems [37, 74].

we have constructed is stable up to a point where the solution branch disappears in a saddle-node bifurcation, and that there is no earlier exchange of stability with a secondary bifurcating branch of solutions or otherwise. Thus from the construction of solutions to the steady state problem and the numerical simulations we are able to deduce features of the bifurcation structure of the underlying reaction-diffusion equation. Furthermore, in Chapter 4 we extended the symmetry argument to the full PDE system (rather than considering only the time-independent problem) and so we expect the same stability properties for solutions of higher pattern mode.

The bifurcation structure elaborated here explains the hysteretic behaviour reported in the previous chapter. On increasing γ the transition between solution branches occurs at the saddle-node point. However, on decreasing γ there is no reason why the reverse transition should take place at this same value of γ which does not correspond to a bifurcation point of the higher mode solution, or indeed that the downward transition should find the original primary bifurcation branch.

We have computed the critical values γ^c for the transition from lowest mode. The critical value of γ for any higher mode m is then determined from the symmetry analysis to be $m^2\gamma^c$. The analytical expressions that we have constructed are approximations to the lowest-mode pattern with negative polarity. Our arguments might just as easily be based on patterns of positive polarity, where the outer part of the lowest-mode solution would be determined by equation (5.9) with $h(u)$ given by the expression (5.11). Similarly, we have chosen a pure kinetic scheme such that solutions for activator and inhibitor are in phase, but could equally have chosen cross kinetics for the cubic autocatalysis model by swapping the signs of the two off-diagonal elements of the matrix $\mathcal{A}$ given in (5.28). The construction of solutions to the piece-wise linear problem in the limit of small d and the analyses for pattern transitions on the growing domain would follow with only minor modifications in this case.

For the kinetic scheme we have considered, heterogeneous solutions bifurcate from the homogeneous steady state as patterns of initially infinitesimal amplitude in a supercritical bifurcation. This was not required for the analysis. Transition-layer solutions with different behaviour on the growing domain can be generated by relaxing the condition that the kinetics admit the Turing bifurcation. In this case we no longer require the fixed point of the kinetics to lie on the middle (unstable) branch of the nullcline. When the kinetic steady state falls on one of the stable branches, either by changing g or shifting the u-nullcline ($f = 0$), sufficiently large amplitude perturbations of the homogeneous solution (now locally stable to small amplitude perturbation) are required to produce large amplitude patterns, which can be constructed in the limit as we have described. However, if the extremal point of the solution on the v-nullcline (at the domain boundary) reaches the fixed point then it will remain at this point, also fixing the value at the other boundary, even as γ increases with domain growth. Then pattern transition at *either* of the turning points is precluded and the pattern

mode will remain unchanged on the growing domain (although the transition-layer region may move and will get progressively narrower on the unit interval).

Many of the models in the literature for biological pattern formation, including the Schnakenberg and Gierer-Meinhardt models discussed in previous chapters, generate spike-type patterns. Some analysis has already been carried out on spike solutions to reaction-diffusion equations, where the form of the nullclines and accordingly the asymptotic structure is different and somewhat less transparent than for the transition-layer phenomena. In the following sections we consider some of the asymptotic properties of spike solutions, in particular the dependence of solutions on γ.

5.6 Analysis of Spike Patterns

Large amplitude patterns also exist as solutions in systems where the activator nullcline has only one stable branch. Such patterns are characterised by the behaviour of the width and height of the activator peak as $\epsilon \to 0$ where, in contrast to transition-layer patterns, the activator peak amplitude varies as some negative power of ϵ and the peak width is decreasing as ϵ tends to zero. In this section we consider the Schnakenberg kinetic scheme as a paradigm for spike patterns, and therefore we study kinetics of cross-type. However, similar results may be obtained for pure systems (for example the Gray-Scott model, see Doelman *et al.* [33]). Also we will consider a single activator peak located within the domain, rather than simply the transition from low to high concentration, as for the previous case.

Initially we consider the construction of solutions (existence) in the general setting. The outer (5.1)–(5.2) and inner (5.3)–(5.4) scalings follow as before. For the case $\epsilon = 0$ then as before the activator v is governed by

$$v_t = g(u, v) \tag{5.83}$$

where the nullcline $g(u, v) = 0$ has two branches; $v = k_i(u)$ for $i = 1, 2$, where only branch $i = 1$ is stable (in comparison with the transition-layer problem there is no stable branch $v = k_3(u)$). For cross kinetics, to generate spike solutions[5] we require that $k_1(u)$ is defined for $u \in (-\infty, u_{max}]$ and $k_2(u)$ is defined for $u \in (\infty, u_{max}]$. In fact for the Schnakenberg system (and many others) $k_2(u)$ is defined on $u \in [u_\infty, u_{max}]$ where, as $v \to \infty$, u tends to the asymptote $u \to u_\infty$, but this will not be important for existence arguments. Furthermore, under the conditions required for the kinetics to admit the Turing bifurcation, the kinetic steady state (u_s, v_s) must lie on the unstable branch $i = 2$. As for transition-layer patterns, the outer solution lies on the stable part of the v-nullcline $g(u, v) = 0$, here branch $i = 1$. The outer solution is governed by

$$0 = u_{xx} + \gamma f\big(u, k_1(u)\big) \tag{5.84}$$

[5] rather than inverted spikes, or *gullies*, see later discussion.

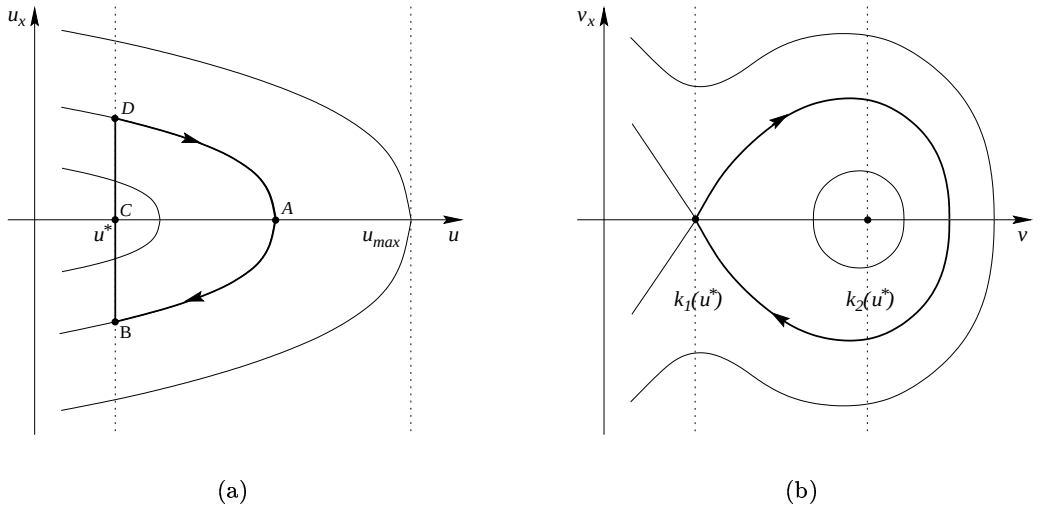

FIGURE 5.9 Schematic of the phase plane for the (a) outer and (b) inner problems for spikes with cross kinetics. In (a) the centralised peak corresponds to the trajectory A to B and then at $u = u^*$ a jump to D, returning to A where $u = u(0)$ at A ($\equiv u(1)$) for symmetric steady solutions. Increasing γ corresponds to larger orbits such that $u(0)$ is increasing with γ (for pure schemes the figure is effectively reflected in $u = 0$ and then $u(0)$ is decreasing with γ). The jump from B to D represents a discontinuity in u_x which corresponds to an excursion in the inner variable, shown in (b), where spikes are homoclinic orbits in (v, v_x).

which is valid away from the location of the spike, $x = x^*$, where $u = u^*$. The phase plane for equation (5.84) is shown schematically in Figure 5.9(a). The function $f(u, k_1(u))$ has no roots and, for cross kinetics, is everywhere positive so that trajectories in the (u, u_x) resemble the form shown in the figure.

In the limit $\epsilon \to 0$ there is a discontinuity in u_x across the spike (where u is continuous). Multiplying equation (5.84) by u_x and integrating we have

$$u_x = \pm\sqrt{2\gamma\big(H(u(0)) - H(u)\big)} \tag{5.85}$$

where $H(u)$ is defined, equivalently to equation (5.13), by

$$H(u) = \int_0^u f(w, k_1(w))\,\mathrm{d}w \tag{5.86}$$

and $u(0)$ is the inhibitor concentration at the left-hand boundary, where $u_x = 0$. Given that $f(u, k_1(u)) > 0$ (and is a monotonically decreasing function of u), $H(u)$ is positive and monotonically increasing and for real values of u_x we must have $u(0) \geq u(x)$ everywhere on the domain (and similarly for $u(1)$) so that u is maximised at the boundaries. Hence $|u_x|$ increases away from the boundaries and is greatest at the spike, where $u = u^*$. Thus u_x takes opposite signs on either side of the peak and the jump in the gradient across the spike is

$$\Delta u_x = 2\sqrt{2\gamma\big(H(u(0)) - H(u^*)\big)} \tag{5.87}$$

and hence u_x is discontinuous.

For $\epsilon \neq 0$ we require a connecting trajectory to smooth out the discontinuity, which is found by expanding in the inner variable $\xi = x/\epsilon$, giving

$$0 = V_{\xi\xi} + \gamma g\left(u^*, V\right) \tag{5.88}$$

which has two fixed points, a saddle point at $(V, V_\xi) = \left(k_1(u^*), 0\right)$ where $g_v < 0$ and a centre at $\left(k_2(u^*), 0\right)$ where $g_v > 0$. The centre is preserved for the nonlinear problem due to the symmetry about $V_\xi = 0$. We seek a solution which for periodic patterns takes us from, and returns us to, the vicinity of the point $\left(u^*, k_1\left(u^*\right)\right)$, which is an orbit in the (V, V_ξ) phaseplane homoclinic to the saddle at $V = k_1(u^*)$. The phase plane for the inner problem is shown schematically in Figure 5.9(b).

In this way, by matching solutions for the inner and outer problems, we can show the existence of large amplitude solutions in the form of spikes in the activator concentration. Next we construct such solutions for the Schnakenberg problem. The time-independent reaction-diffusion problem with Schnakenberg kinetics, where the kinetic parameter a is small,[6] is given by

$$0 = u_{xx} + \gamma\left(b - uv^2\right) \tag{5.89}$$

$$0 = \epsilon^2 v_{xx} + \gamma\left(\epsilon^\beta \hat{a} + uv^2 - v\right) \tag{5.90}$$

where $\beta > 0$. It is convenient to consider single spike solutions on the interval $[-1, 1]$, with zero flux conditions at the boundaries. The symmetry of the time-independent problem, as discussed in Chapter 2, and in particular the symmetry of these equations under $x \to -x$ suggests that we look for a spike centred at $x^* = 0$.[7] Half-peak solutions follow immediately by considering the interval $[0, 1]$.

Taking a regular series expansion for the outer region in variable x

$$u(x, \epsilon) = \sum_{j=0}^{\infty} \epsilon^j u^{(j)}(x), \qquad v(x, \epsilon) = \sum_{j=0}^{\infty} \epsilon^j v^{(j)}(x) \tag{5.91}$$

to leading order we have

$$u^0_{xx} = \gamma b \tag{5.92}$$

$$0 = u^0 (v^0)^2 - v^0 \tag{5.93}$$

with zero flux boundaries, which is solved to obtain

$$v^0 = 0 \tag{5.94}$$

$$u^0(x) = \gamma b\left(|x| - \frac{1}{2}x^2\right) + c \tag{5.95}$$

[6] The analysis follows with only minor modifications for $a \sim \mathcal{O}(1)$.

[7] Determination of the location of the *transition-layer* was found to be nontrivial, and is equivalent to finding the *width* of the activator peak. For spike patterns the width of the peak tends to zero with ϵ, and the location is assumed from symmetry arguments, thus no further assumptions are made here than were employed for the transition-layer problem.

where c is a constant.[8]

Expanding about the peak by introducing the inner variable $\xi = x/\epsilon$ (for $x^* = 0$), the inner region is governed by

$$0 = U_{\xi\xi} + \epsilon^2\gamma\left(b - UV^2\right) \tag{5.96}$$

$$0 = V_{\xi\xi} + \gamma\left(\epsilon^\beta \hat{a} + UV^2 - V\right) \tag{5.97}$$

and again seeking a regular expansion

$$U(\xi,\epsilon) = \sum_{j=0}^{\infty} \epsilon^j U^{(j)}(\xi), \qquad V(\xi,\epsilon) = \sum_{j=0}^{\infty} \epsilon^j V^{(j)}(\xi) \tag{5.98}$$

we find to leading order

$$U^0_{\xi\xi} = 0 \tag{5.99}$$

$$V^0_{\xi\xi} = \gamma(V^0 - U^0(V^0)^2). \tag{5.100}$$

Given that we do not want U^0 to blow up as $U \sim 1/\epsilon$ away from the spike, we choose U^0 to be constant,

$$U^0 = u^*, \tag{5.101}$$

which may depend on γ. Solving equation (5.100) for V^0 we find

$$V^0(\xi) = \frac{3}{2u^*}\operatorname{sech}^2\left(\frac{\xi\sqrt{\gamma}}{2}\right) \tag{5.102}$$

which is in the form of a spike, homoclinic to $(V, V_\xi) = (0,0)$ for $\xi \in [-\infty, \infty]$. Matching inner to outer solutions is automatic for v and for u we find $c = u^*$ so that the leading order composite solutions are

$$u(x) \sim u^* + \gamma b\left(|x| - \frac{1}{2}x^2\right) \tag{5.103}$$

$$v(x) \sim \frac{3}{2u^*}\operatorname{sech}^2\left(\frac{x\sqrt{\gamma}}{2\epsilon}\right). \tag{5.104}$$

Previously, for the transition-layer problem, we have evaluated the constant inhibitor concentration, u^*, for the inner solution with the integral condition (5.20), $G(u^*) = 0$, which requires that the gradient V_ξ tends to zero away from the inner region. However, we have effectively used this condition in the integration of equation (5.100), from which we deduce the form of the spike (5.102). For activator spike amplitude v_{pk} then the integral is

$$G(u^*) = \int_0^{v_{pk}} g(u^*, w)\, \mathrm{d}w = 0. \tag{5.105}$$

[8] Therefore we have $\mathrm{d}u(x)/\mathrm{d}\gamma \geq 0$ everywhere on the domain, and particularly at the boundaries, and hence $u(0)$ is an increasing function of γ here.

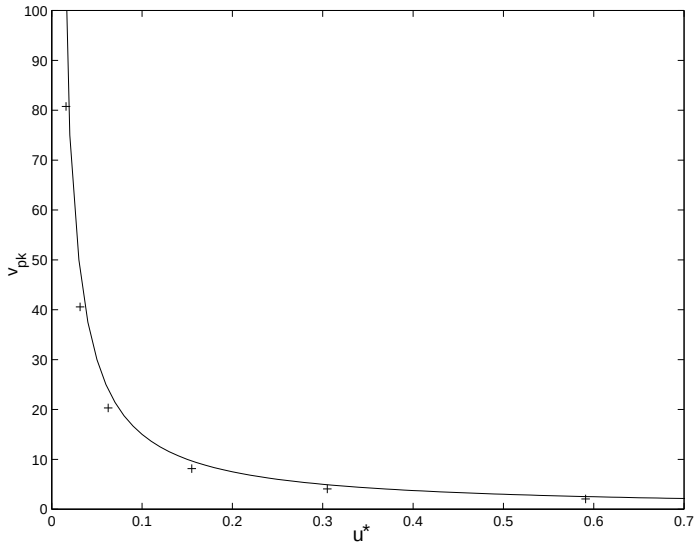

FIGURE 5.10 The relationship between activator amplitude v_{pk} and inhibitor concentration u^* in spikes for Schnakenberg kinetics. The solid line shows the analytical expression (5.106) and the crosses show values obtained from numerical simulations for different values of ϵ, with ϵ decreasing from right to left.

Evaluating the integral (for small a) we recover simply

$$v_{pk} = \frac{3}{2u^*} \tag{5.106}$$

which is consistent with our composite solutions. We plot this relation in Figure 5.10, along with data obtained from numerical simulations for different values of ϵ, showing close agreement to the analytical curve. However, thus far we have assumed uniform expansions for the dependent variables which, from this figure, are not $\mathcal{O}(1)$ in the inner region. This suggests that we rescale the equations to find variables which are $\mathcal{O}(1)$ before taking the expansion in ϵ. The following scaling of the equations is similar to one used in a recent paper by Doelman *et al.* [33] who consider the spike solutions in the Gray-Scott model.

We consider general scalings for the various terms in the inner equations, writing

$$u = \epsilon^{\alpha}\hat{u}, \quad \text{and} \quad v = \epsilon^{-r}\hat{v} \tag{5.107}$$

where $\alpha, r \geq 0$. The time independent activator equation (5.4) becomes

$$0 = \hat{v}_{\xi\xi} + \gamma\left(\epsilon^{(\beta+r)}\hat{a} + \epsilon^{(\alpha-r)}\hat{u}\hat{v}^2 - \hat{v}\right). \tag{5.108}$$

To obtain solution in the form of a homoclinic orbit of the saddle point we must have balance between the final two terms (otherwise the equation is linear and certainly will not admit such a solution). Thus we require $\alpha = r$, and we seek an inner solution

$(\hat{U}(\xi), \hat{V}(\xi))$ for the equations

$$0 = \hat{U}_{\xi\xi} + \epsilon^{2(1-\alpha)}\gamma\left(\epsilon^{\alpha} b - \hat{U}\hat{V}^2\right) \tag{5.109}$$

$$0 = \hat{V}_{\xi\xi} + \gamma\left(\epsilon^{(\alpha+\beta)}\hat{a} + \hat{U}\hat{V}^2 - \hat{V}\right). \tag{5.110}$$

For $0 \leq \alpha < 1$ we have $\epsilon^{2(1-\alpha)}$ is small and the equations decouple (giving distinguished subsystems describing inner and outer regimes). For $\alpha > 1$, then from (5.109) we must have $\hat{U} = 0$ for which there is no homoclinic solution for $\hat{V}$. If, however, $\alpha = 1$ then we recover a coupled second order ODE system for the inner region, so that in the asymptotic limit the problem does not simplify in the manner described above.

If we assume that $0 \leq \alpha < 1$, then expanding in powers of $\epsilon^{(1-\alpha)}$

$$\hat{U}(\xi, \epsilon) = \sum_{j=0}^{\infty} \epsilon^{(1-\alpha)j}\, \hat{U}^{(j)}(\xi), \qquad \hat{V}(\xi, \epsilon) = \sum_{j=0}^{\infty} \epsilon^{(1-\alpha)j}\, \hat{V}^{(j)}(\xi) \tag{5.111}$$

we recover the same leading order problem as was solved above, for which $\hat{U}^0$ is constant, as in (5.101), and $\hat{V}^0$ is given by (5.102). Matching to the leading order expressions for the outer problem, the composite solutions are

$$u(x) \sim \epsilon^{\alpha} u_0^* + \gamma b\left(|x| - \frac{1}{2}x^2\right) \tag{5.112}$$

$$v(x) \sim \epsilon^{-\alpha} \frac{3}{2u_0^*} \operatorname{sech}^2\left(\frac{x\sqrt{\gamma}}{2\epsilon}\right) \tag{5.113}$$

showing the scaling of the spike width and amplitude with ϵ.

From this analysis we are not able to evaluate the parameter α, which determines the scaling with ϵ. In fact for Schnakenberg kinetics numerical simulations suggest that the correct scaling in the inner region is $\alpha \approx 1$, the situation in which there is no simplification of the time-independent equations. Nevertheless, we can compare the form of our approximate analytical solutions to the results of numerical simulations by taking the numerical value of v_{pk} and calculating u^* accordingly. In Figure 5.11 we compare the analytical expressions (5.112) and (5.113) to numerical solutions for two values of ϵ. From these figures and from the part of the composite solutions on the unit interval $[0, 1]$ we may recover a mode $m = 1$ (half-peak) approximation. However, it is apparent that the composite solution is not uniformly valid in this case, as the zero-flux boundary condition for the inhibitor u is not satisfied at $x = 0$, where the half-spike is located, as the gradient in the inhibitor u_x is discontinuous (and hence ill-defined) here. It is for this reason that we chose to construct a centralised spike on $[-1, 1]$. For $\epsilon \neq 0$ the discontinuity in u_x is removed and the boundary condition can be satisfied, so that the half-peak is a valid solution of the steady state problem.

5.6.1 Splitting and Insertion. The mechanism described previously for transitions between quasi-steady patterns under slow uniform domain growth is sufficient to explain transitions via peak insertion for spike patterns, demonstrated for Gierer-Meinhardt kinetics in Figure 4.10(a). Here $u(0)$ (the boundary value of u) increases

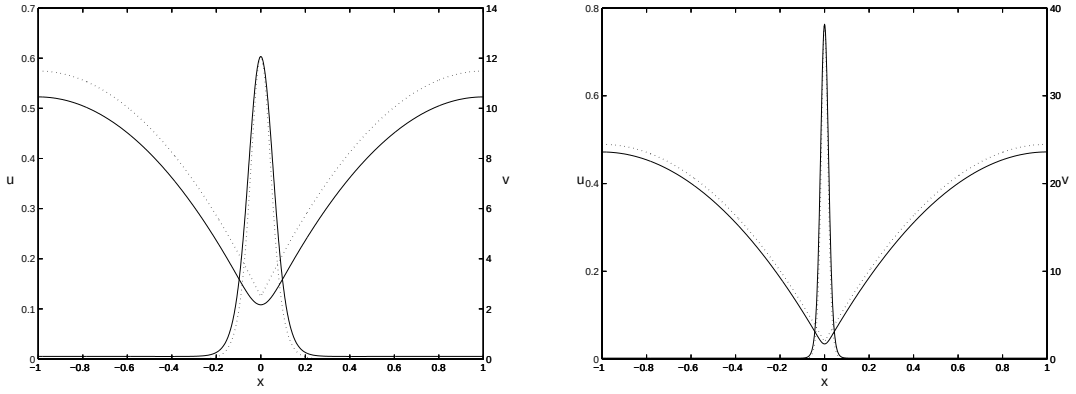

(a) (b)

FIGURE 5.11 Numerical solution (solid) and asymptotic approximation (5.103)–(5.104) (dotted) for spike solutions with Schnakenberg kinetics for two values of ϵ. We plot steady state solutions with $\gamma = 4.0$ and (a) $\epsilon \approx 0.0316$ ($d = 0.001$) while in (b) $\epsilon = 0.01$ ($d = 0.0001$). Note the different scales on the u and v axes.

with γ until reaching u_{max} at the critical value of γ. At this point v locally increases rapidly, giving a pattern transition on the fast timescale by activator peak insertion. Similarly, spike systems with pure kinetics for which the v-nullcline has a stable branch $v = k_1(u) \in [u_{min}, \infty)$ and an unstable branch $v = k_2(u) \in [u_{min}, \infty)$ undergo activator peak insertion when $u(0)$, now decreasing with γ, reaches u_{min}, beyond which the solution ceases to exist.

However, our numerical simulations have shown that spike-type patterns may demonstrate both peak insertion and peak splitting on the growing domain. Spike splitting is realised for Schnakenberg kinetics, shown in Figure 4.1(a). For transition-layer patterns the mechanisms for splitting and insertion are essentially equivalent. From the differences in the nullclines and, correspondingly, in the asymptotic behaviour of spike and transition-layer solutions, it is evident that an explanation of spike splitting must take a different form. This is due to the fact that spikes are homoclinic orbits in the (v, v_x) plane, and do not connect two distinct branches of the v-nullcline, as do transition-layers. However, a similar explanation in terms of the existence of solutions as γ increases might be expected. In fact, plotting spike solutions in the (u, v) plane one notices that the approximation of constant u in the spike region becomes less and less reasonable as γ increases. This suggests that the essential features responsible for spike splitting may not be captured in the leading order expansion. Various other authors have sought to understand spike splitting, following the observation of splitting phenomena in the Gray-Scott model, as discussed in Chapter 2. Doelman *et al.* [33] study two-pulse solutions to the Gray-Scott model and consider existence and stability results for pairs of pulses on the unbounded domain.

They identify the region of parameter space in which one-pulse solutions cease to exist and show numerically that the self-replication process may occur in the vicinity of the boundary of the stable one-pulse region. Further, they find that a pair of pulses will separate with decreasing velocity, and evolve towards one of the stable multi-peak solutions which act as attractors during the self-replication process. Reynolds *et al.* [116] consider the splitting of moving pulses in terms of the balances of flux into the spike region. However, at present we know of no transparent explanation of the splitting of static spikes.

5.6.2 Pattern Sequences in the Gierer-Meinhardt Model. In the previous chapter we noted that the kinetic model proposed by Gierer and Meinhardt, equations (4.29)–(4.30) (see Appendix A.3), can give a singular solution behaviour on the growing domain, where transition between pattern modes appears to be precluded, by setting the constant term in the activator kinetics, δ, to zero. For non-zero values, pattern sequences are formed as usual, via activator peak insertion. These two behaviours are illustrated in Figure 4.10.

For non-zero δ the v-nullcline is given by

$$u = \frac{\nu_2 v^2}{\mu_2 v - \delta} \tag{5.114}$$

where ν_2 and μ_2 are positive constants. Thus we have the standard arrangement in the phase plane for pure kinetics with stable $u = k_1(v)$ and unstable $u = k_2(v)$ branches defined on $u \in [u_{min}, \infty)$, where u_{min} is the minimum value of (5.114). Insertion of new peaks in the activator concentration profile occurs when $u(0)$, decreasing as γ increases (for pure kinetics) reaches this minimum value. However, when δ is identically zero, the v-nullcline becomes

$$v = 0 \tag{5.115}$$

$$u = k_2(v) = \frac{\nu_2}{\mu_2} v \tag{5.116}$$

where the former is the stable branch. Therefore, in the limit $\epsilon \to 0$, the outer part of the solution lies on $v = 0$ in the phase space, and as γ increases $u(0)$ decreases towards $u(0) = 0$. However, in the fast timescale, $u(x,t)$ is governed by the equation

$$u_t = \frac{1}{\gamma} u_{xx} + \nu_1 v^2 - \mu_1 u \tag{5.117}$$

where ν_1 and μ_1 are positive constants. In the outer regime v is exponentially small (and for $\epsilon = 0$ then $v = 0$). For zero flux conditions u is a minimum at the boundary and so the second spatial derivative near the boundary is positive. Therefore the time derivative at the boundary is bounded from below by

$$\frac{\mathrm{d}u(0)}{\mathrm{d}t} = -\mu_1 u(0) \tag{5.118}$$

and for finite time $u(0)$ is bounded away from zero. Thus the quasi-steady solutions never obtain the minimum value for u for any finite value of γ and the critical point for insertion is never reached. For any non-zero δ then the minimum point moves away from $u = 0$ and we recover insertion as γ increases through its critical value.

The somewhat surprising implication of this result is that the initial pattern mode established from random initial data must persist with slowly increasing γ. We have identified the critical point in γ as the point at which the solution ceases to exist and hence infer that for $\delta = 0$ the solution branch exists for all γ. Furthermore, for different choices of initial domain length and initial data, any pattern mode may be established initially and so this result holds for all pattern modes (this is also evident from the scaling of different solution branches with γ as discussed in Chapter 2). Finally, we have performed numerical simulations in which we added small amplitude random noise to the solution at each integration timestep and found that the pattern appears to remain stable with increasing γ. This singular property of the solutions when $\delta = 0$ may be important as several authors (see for example Ni [92]) ignore the constant terms when investigating the behaviour of solutions to the Gierer-Meinhardt equations.

5.6.3 Piece-wise Linear Spikes. The necessary ingredients for spike solutions presented at the start of this section suggest that spikes should be possible in a piece-wise linear kinetic scheme with the requisite features of the nullclines. To this end we investigate solutions of the piece-wise linear scheme introduced in section 5.2 when the gradient of activator nullcline in region $i = 3$ is varied.

To expedite comparison to the cross-kinetic Schnakenberg system, we study piece-wise linear kinetics of cross-type

$$f(u,v) = -\sigma u - v \tag{5.119}$$

$$g(u,v) = g_i = \left\{ \begin{array}{l} g_1 \\ g_2 \\ g_3 \end{array} \right. = \left\{ \begin{array}{ll} u - \eta(v + 2\theta_1), & v < -\theta_1 \\ u + \eta v, & -\theta_1 \leq v \leq \theta_3 \\ u - \phi\eta(v - \theta_3) + \eta\theta_3, & v > \theta_3 \end{array} \right. \tag{5.120}$$

where we have introduced the parameter ϕ which will be varied to change the gradient of the second stable branch of the v-nullcline, shown in Figure 5.12(a) for various choices of ϕ. The corresponding steady state numerical solutions for the half-peak located at the right-hand boundary are shown in Figure 5.12(b). As ϕ is changed from positive to zero and then to negative values, such that there are two and then only one stable branches, the asymptotic behaviour of the solutions changes from transition-layer to spike type, as expected.

The natural transition behaviour for this system on growing domains is to undergo transitions by insertion of new activator peaks, shown in Figure 5.13(a), resembling the pattern sequence in the Gierer-Meinhardt model. However, if θ_3 is also allowed to vary, the splitting of peaks may be recovered for the piece-wise linear problem when θ_3

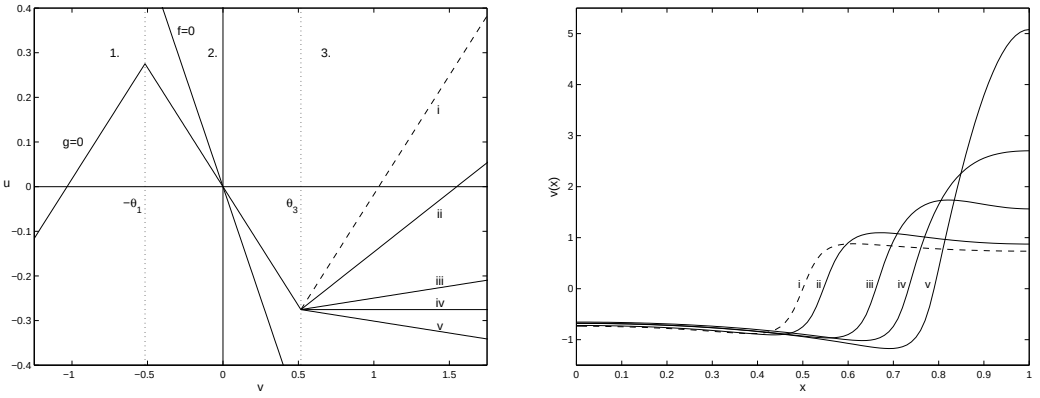

(a) (b)

FIGURE 5.12 Spike solutions in the piece-wise linear model (5.119)–(5.120): evolution from transition-layers to spikes as the second stable branch is removed. We use cross kinetics with $\sigma = 1.0$, $\mu = 0.8$ (so that $\eta = 2\mu/3 \approx 0.533$) and $\theta_{1,3} = \pm\sqrt{\mu/3}$. The nullclines are shown in (a) for (i) $\phi = 1.0$ (dashed line, as previously studied), (ii) $\phi = 0.5$, (iii) $\phi = 0.1$, (iv) $\phi = 0$ where the branch is no longer stable and (v) $\phi = -0.1$. The corresponding steady state solution profiles for the activator v are plotted in (b) with $d = 0.01$ and $\gamma = 1.0$, showing the transition to spike-type solutions as ϕ decreases through zero.

is reduced towards zero, illustrated in Figure 5.13(b). Further analysis of these pattern sequences has not been carried out, however, the simplification in the analysis of the equations engendered by the introduction of the piece-wise linear approximation may yield an understanding of the peak splitting phenomenon in spike solutions.

We have only considered the case when the homoclinic orbit in the (v, v_x) plane produces a spike increasing in v. If, however, the v-nullcline is the other way up in the phase space, so that for cross kinetics the unstable, $v = k_1(u)$, and stable, $v = k_2(u)$, branches are defined for $u \in [u_{min}, \infty)$, then inverted spikes or *gullies* are formed. Similarly, this is the case for pure kinetics where the two branches of the v-nullcline are defined on $u \in (-\infty, u_{max}]$. The results of a numerical simulation for such a kinetic scheme are shown in Figure 5.13(c), where for slow domain growth the solution undergoes splitting of the plateaus of high activator concentration (or, equivalently, insertion of new gullies). Similarly, it should be possible to vary the nullclines such that the gullies split as the domain grows (and new activator plateaus are inserted). We do not know of any nonlinear kinetic schemes proposed in the literature which generate these types of patterns, however, this behaviour is generic to the class of reaction terms with nullclines of the form that we have described.

5.6.4 Discussion. The investigation of spike solutions has raised several interesting questions. Firstly, during the construction of spike solutions to the Schnakenberg model in the asymptotic limit $\epsilon \to 0$ we found that the formal expansion was only

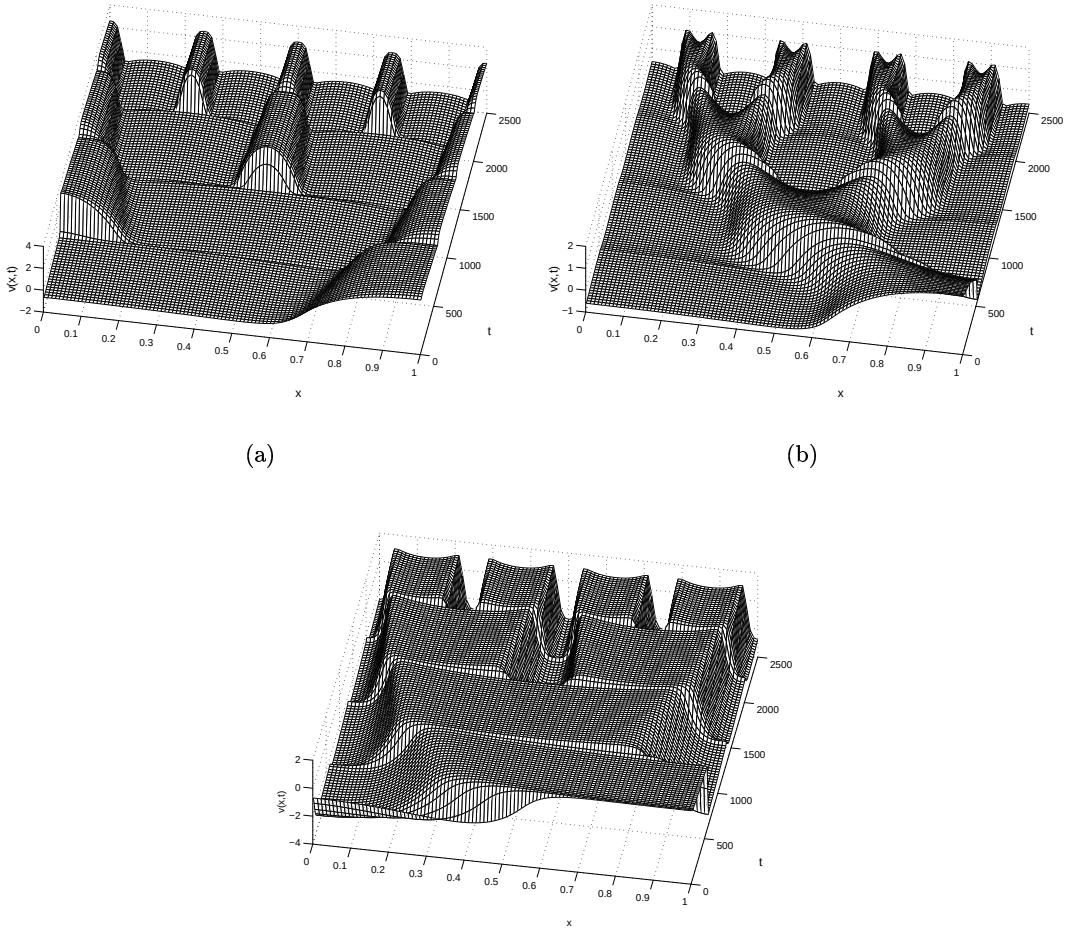

FIGURE 5.13 Spike splitting and insertion in the piece-wise linear kinetic model (5.119)–(5.120) with $\sigma = 1.0$ and $\mu = 0.8$ ($\eta = 2\mu/3 \approx 0.533$). We take $\phi = -0.01$ and (a) $\theta_3 = \theta_1 = \sqrt{\mu/3}$ while in (b) $\theta_3 = \theta_1/10$. In (c) the parameters are as for (a) but we have transformed the kinetics under $(u, v) \to (-u, -v)$.

valid for $0 \leq \alpha < 1$. This parameter cannot be found analytically, however, numerical simulations suggest $\alpha \approx 1$. Despite this apparent contradiction, the analytical solutions give a good approximation to numerical simulations (see Figure 5.11). Secondly, although insertion of activator peaks (and the failure to do so when $\delta = 0$) in the Gierer-Meinhardt model can be well understood, the analysis that we have presented does not give an explanation for spike splitting, as realised for Schnakenberg kinetics. Furthermore, numerical simulations suggest that the leading order inner approximation, where u is constant, is not sufficient to understand the phenomenon. The piece-wise linear model that we have described may prove useful as a simplified system in which to explore this behaviour.